University of South-Eastern Norway

www.usn.no

FMH606 Master's Thesis 2021

Process Technology

Pyrolysis of biomass

Ahmad Dawod

Faculty of Technology, Natural sciences and Maritime Sciences
Campus Porsgrunn

University of South-Eastern Norway

www.usn.no

Course: FMH606 Master's Thesis, 2021

Title: Pyrolysis of biomass

Number of pages: 81

Keywords: Pyrolysis, Wood pellets, Operational conditions, Computational Particle Fluid Dynamic (CPFD), Biomass air gasification

Student: Ahmad Dawod

Supervisor: Britt M. E. Moldestad

Hildegunn H. Haugen

Janitha Bandara

Availability: Open

University of South-Eastern Norway

www.usn.no

Summary:

Pyrolysis of biomass is considered to be a green technology since it has no impacts or emissions to the environment. Pyrolysis of biomass is the initial stage in the gasification process and is defined as the thermal decomposition of biomass into valuable products such as char, tar, and gas. In this study, a pyrolysis reactor was designed and constructed, and experimental tests were performed to study the pyrolysis products, especially the gas compositions. An extensive literature study has been carried out on the pyrolysis of biomass along with the effects of different operational conditions on the product yields. Further, computational particle fluid dynamic (CPFD) simulations were performed to study the composition of the synthesis gas obtained from the gasification of wood pellets.

The pyrolysis experiment was performed using wood pellets as the feedstock and the reactor temperature was set to 500°C. The product yields were found to be 29.24%, 22.48%, and 48.28% for char, tar, and gas, respectively. The char yield was within the range compared to the literature, while the tar yield was lower, and the gas yield was significantly higher. The deviation is mainly due to experimental uncertainty, where condensable tar escaped with the gas. Gas samples were further analyzed by a gas chromatograph (GC) and the average gas compositions were 62.02%, 6.73%, and 33.15% for cumulative CH_4 and CO, H_2, and CO_2, respectively. The results agreed well with the results from the literature, especially for H_2 and CO_2.

A CPFD model was created using the Barracuda Virtual Reactor 17.4.1 software. Three simulation cases were created by varying the reactor temperature and pyrolysis gas compositions. The effect of the pyrolysis step was found to be significant, especially on the production of CO, H_2, and CH_4. This is mainly because 85 wt.% of the synthesis gas was produced during the pyrolysis stage.

Comparing the simulation results with the experimental results showed a good agreement on predicting CH_4 and H_2 while overestimation of CO_2 and underestimation of CO was observed. This might be due to errors in the pyrolysis gas composition or high rates in the water-gas-shift reaction.

The effects of temperature on the synthesis gas composition were further investigated. Increasing the temperature increased the concentration of CO and H_2 by 2.4% and 1.6% respectively, while decreased the concentration of CO_2 and CH_4 by 1.3% and 0.5%, respectively. The result trends show a good agreement with other experiments from the literature, except the trend of CH_4. This might be due to the neglect of the tar composition in the volatiles.

Preface

This thesis was completed in the spring semester of 2021 as a fulfillment of a partial requirement to achieve a master's degree in Process Technology at the University of South-Eastern Norway.

I would like to thank my supervisors Britt M. E. Moldestad, Janitha Bandara, and Hildegunn H. Haugen for their guidance, support, and help through this project.

Porsgrunn, 2021

Ahmad Dawod

Contents

List of figures

List of tables

Nomenclature

Abbreviations	**Explanations**
CAD	Computer-Aided Design
CFD	Computational Fluid Dynamic
CFX	Computational Fluid dynamics program
CPFD	Computational Particle Fluid Dynamic
FID	Flame Ionization Detector
GC	Gas Chromatograph
HHV	Higher Heating Value
IPA	Isopropyl Alcohol
LHV	Lower Heating Value
MP-PIC	Multiphase Particle-In-Cell
MSW	Municipal Solid Waste
TCD	Thermal Conductivity Detector
USN	University of South-Eastern Norway
VR	Virtual Reactor
Chemical compound	**Explanations**
C	Carbon
C_2H_2	Acetylene
C_2H_4	Ethylene
C_2H_6	Ethane
C_6H_6	Benzene
CH_4	Methane
CO	Carbon monoxide

CO_2	Carbon dioxide	
H_2	Hydrogen	
H_2O	Water	
He	Helium	
N_2	Nitrogen	
O_2	Oxygen	
SiO_2	Sand	
Symbol	**Explanations**	**SI Unit**
k_1, k_2, and k_3	Rate constants	[s^{-1}]
M_C	Mass of char	[kg]
m_{C1}	Mass concentration of primary char	[kg/m^2]
m_{C2}	Mass concentration of secondary char	[kg/m^2]
M_G	Mass of gas	[kg]
m_{G1}	Mass concentration of primary gas	[kg/m^2]
m_{G2}	Mass concentration of secondary gas	[kg/m^2]
M_T	Mass of tar	[kg]
m_W	Mass concentration of wood	[kg/m^2]
PH	Acidity or basicity of a solution	[-]
t	Time	[s]
ΔH	Heat of formation	[kJ/mol]
δ	Yield ratio	[-]

1 Introduction

This chapter covers the background and the objectives of the thesis, along with different methods for waste treatment.

1.1 Background

Waste generation has increased greatly around the planet in ongoing many years, and there are no signs of its decline. The world generates 2.01 billion tons of municipal solid waste (MSW) every year [1]. According to the World Bank estimation, the overall waste generation will increase by around 70% to 3.4 billion tons by 2050. This is due to various components, such as population growth, urbanization, economic development, and customer shopping habits [2]. At least 33% of the generated waste worldwide is not managed in an environmentally safe way and instead dumped or openly burned [1].

The 2008 EU Waste Framework Directive introduced a waste hierarchy, which sets out the basic concepts and definitions related to waste management. The waste hierarchy illustrated in Figure 1.1 lists prevention at the top (most preferable) to reuse, recycling, energy recovery to the least favored option disposal of waste at the bottom [3].

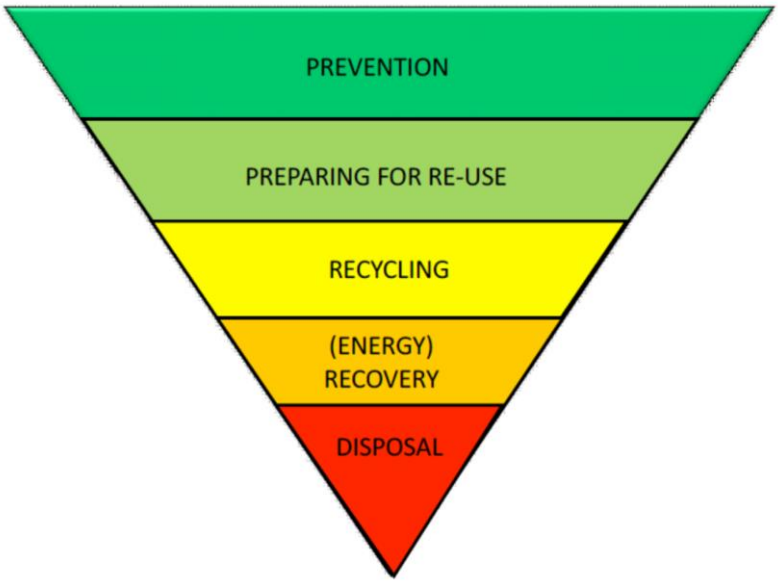

Figure 1.1 Waste hierarchy [4].

CO_2 and other greenhouse gas emissions into the atmosphere contribute to climate change, especially global warming. The concerns about global warming and declining petroleum resources have prompted a move towards renewable energy resources [5]. Biomass is one of the potential feedstocks that satisfies the environmental issues and considered as one of the most important resources in near future [6]. Biomass is defined as any organic non-fossil material and formed by or from living organisms [7]. Compared to other renewable energy sources such as solar, wind, and hydropower, biomass can be converted directly into valuable fuels rather than just generating electricity [5]. Wood-based biomass is one of the most commonly used green energy sources that can be utilized in producing valuable products [8].

Forrest and manufacturing processes wastes are the major sources of wood-based biomass. Around 50% of the wood is processed to timber or other valuable products, while the rest becomes wastes [9].

Several technologies and techniques within waste management have been utilized, whereas some are still under development. The goals are to improve health and protect the environment, and conservation of resources such as material, energy, and space [10]. Treatment techniques are selected and utilized based on the form, composition, and amount of biomass [11]. Thermal treatment processes including combustion, gasification, and pyrolysis, are utilized to convert biomass into valuable products [12].

Pyrolysis of biomass is one of the thermal treatment technologies that break biomass into bio-oil, solid biochar, and gases. Pyrolysis is defined as a process for breaking down the biomass by heating to high temperatures in the absence of oxygen [7]. Bio-oil from pyrolysis is gaining increasing interest due to easier storage and transportation at a lower cost than solid biomass, which can be used as a substitute combustion fuel for power generation and transportation [13]. Biochar can be used for different industrial uses such as solid fuel in boilers and the production of activated carbon. Finally, the gas produced from the pyrolysis of biomass can be used as fuel for industrial combustion or to supply the energy required for the pyrolysis process [12].

1.2 Waste treatment methods and resources

The hierarchy of waste management and the idea of integrated waste management have contributed to the development of waste treatments and disposal technologies, instead of focusing on landfill and incineration methods. The developed treatment technologies have minimal environmental impact and energy recovery with low pollution. Among such technologies are pyrolysis, gasification, combined pyrolysis-gasification, composting, and anaerobic digestion, as illustrated in Figure 1.2 [14]. These technologies convert solid waste into valuable products, chemicals, and fuels. Typical solid waste streams are MSW such as Food, wood, paper, plastics, waste tires, etc. The main products and chemical yields generated from waste treatment facilities include [15]:

1) Liquid fuels such as oil, biodiesel, and ethanol.
2) Electricity, heat, and steam from combustible gases such as methane.
3) Chemicals and consumer products from syngas.
4) Activated carbon.

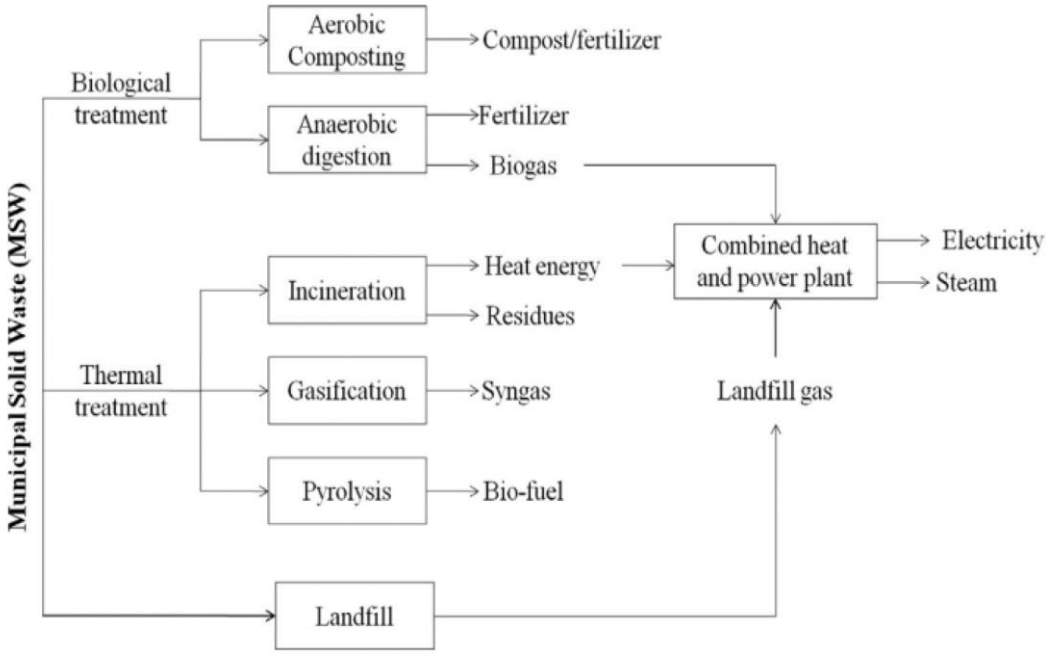

Figure 1.2 Waste treatment methods and their products [16]

Thermal treatment option includes gasification (conversion under high temperature and pressure in a low-oxygen environment to produce fuel gases) and pyrolysis (similar to gasification but in the absence of oxygen). The interest in these options is growing as an environmental and economic alternative for waste treatment [14]. As illustrated in Figure 1.3, the main difference between pyrolysis, gasification, and incineration is the amount of oxygen supplied to each thermal process. For pyrolysis, there is no oxygen supply, while for gasification there is a limited supply of oxygen. Thereby complete combustion does not take place, instead, combustible gases such as carbon monoxide and hydrogen are produced [14].

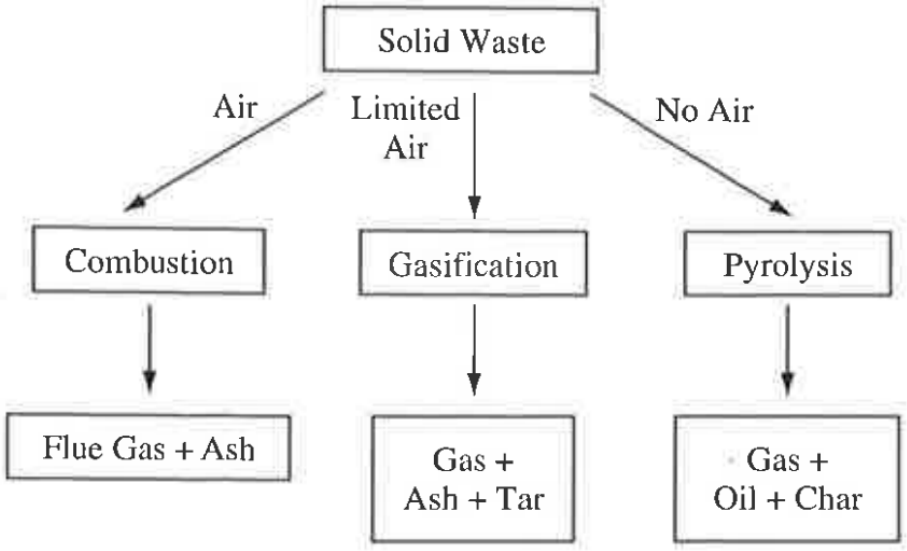

Figure 1.3 Pyrolysis, gasification and incineration [14].

Biological treatment processes such as aerobic composting and anaerobic digestion are also alternative options for the treatment of waste. Biological treatment proceeds at lower temperatures and lower reaction rates than other thermal conversion processes [15]. Aerobic composting is the biological degradation of biodegradable organic waste such as garden and food waste. Composing is a relatively fast method of biodegradation, usually taking between 4-6 weeks to produce a stabilized product. Anaerobic degradation is also an option for the treatment of MSW and other wastes such as sewage sludge, agricultural waste, and animal manure. This method generates the same gases as in landfill sites, gases such as carbon dioxide and methane, but in a controlled, closed environment. whereas the generated gas can be used directly as fuel or converted to a higher quality gaseous fuel or chemical feedstock. Moreover, it is possible to use the residual as a soil conditioner [14] [17].

1.3 Objectives of the thesis

The pyrolysis of biomass into valuable resources is gaining great interest as a feasible and environmentally friendly option for waste treatment. The product yield from pyrolysis of biomass includes biochar, bio-oil, and gases. How much of each product is produced is dependent on the biomass composition and the process conditions. The overall aim is to design and construct a pyrolysis reactor and perform experimental tests to study the product composition of the biomass pyrolysis as a function of biomass type and operational conditions, especially the temperature. Another goal is to simulate a fluidized bed gasification reactor using a computational particle fluid dynamic (CPFD), using actual experimental data from pyrolysis as an input. Task description in detail is attached in Appendix A.

2 Pyrolysis of biomass

This chapter describes the chemical and physical aspects of the pyrolysis mechanism, along with the effects of different operational conditions on the pyrolysis product yields. An overview of biomass resources and pyrolysis reactor design are introduced.

2.1 Biomass resources

Biomass resources, also known as bio-renewable resources, refer to all types of organic non-fossil materials, such as plant, animal, and waste materials [13] [18]. Biomass fuels are classified as environmentally friendly, and the use of biomass for energy production is on the rise. As a result, all available biomass resources are becoming increasingly important [19]. Biomass resources can be divided into five categories: virgin wood, energy crops, agricultural residues, municipal solid wastes, MSW, and industrial wastes [19]. Examples of each category are illustrated in Table 2.1.

Table 2.1 Different resources of biomass [19] [12].

Category	Examples
Virgin wood	Wood, logging residues, branches, sawdust, bark, and wood chips
Energy crops	Short rotation woody crops, herbaceous woody crops, grasses, corn, wheat and barley, sugarcane and beet sugar, soybean, sunflower, safflower
Agricultural residues	Lower quality agricultural products, stalks, straw or husks, animal manure, and animal bedding
Municipal solid wastes (MSW)	Food, wood, paper, cardboard, leather, textiles, and yard trimming
Industrial wastes	Waste from wood, paper, and pulp industries, textile industry, food industry, sewage sludge, and waste oils.

Lignocellulosic biomass refers to woody and grassy plant materials that are mainly composed of cellulose, hemicellulose, and lignin [20]. The biomass type affects the pyrolysis process and its product yields. The relative mass ratios of organic and inorganic components vary depending on biomass type, growth conditions, and harvesting time. Pyrolysis of each constituent has its reaction pathways and thermochemical properties, resulting in different product yields [21].

Woodchips and wood pellets are common pyrolysis feedstocks that fall under the lignocellulosic biomass classification. Woodchips are typically high in moisture content and are made by cutting wood into small pieces ranging from 1 to 5 cm. Wood pellets are made from dried, pressed and finely grounded wood chips, with a typical particle size of 3.2 - 6.4 mm [19] [22].

There are other biomass feedstocks such as macroalgae and seaweed that are not sufficiently explored for pyrolysis. Macroalgae is a fast-growing marine organism classified as non-lignocellulosic biomass. Macroalgae contain low levels of cellulose and lignin and are instead composed of elastic polysaccharides (laminarin, carrageenan, agarose, and alginic acid) and free sugars (mannitol and fucoses). As a result, macroalgae could be a possible option for pyrolysis with an available biomass supply across the world [23] [24].

2.1.1 Ultimate and proximate analysis of biomass

The chemical composition of the biomass has a major impact on the chemistry of pyrolysis [25]. The ultimate analysis evaluates the mass percentages of individual elements within biomass such as Carbon, hydrogen, nitrogen, and oxygen [26]. The proximate analysis gives the gross components of the biomass such as moisture, volatile matter, ash, and fixed carbon. The proximate analysis gives a good idea of the percentages of the main pyrolysis product yields [25]. The volatile matter of biomass is the condensable vapors and non-condensable gases emitted when biomass is heated [22]. Fixed carbon represents the amount of solid carbon that remains in the char after pyrolysis, and ash is the inorganic solid residue that remains after complete combustion of the biomass [22] [26].

2.2 Principles of pyrolysis

Pyrolysis is defined as the thermal degradation of biomass in the absence of oxygen and the presence of nitrogen [14]. The term derives from two Greek words: pyro, meaning fire, and lysis, meaning disintegration into integral parts [27]. Pyrolysis is typically performed at low temperatures ranging between 400-800°C compared to 800-1000°C for gasification [14]. The pyrolysis process is endothermic, which means that it needs a heat supply to the reactor [28]. The product yield from pyrolysis of biomass is classified into three types, presented in Table 2.2:

Table 2.2 Product yields from pyrolysis of biomass [22].

Phase	Products
Solid	Biochar or carbon
Liquids	Tars or bio-oil, heavier hydrocarbons, and water
Gases	mainly CO_2, CO, CH_4, H_2, H_2O, and other lighter hydrocarbons such as C_2H_2, C_2H_4, C_2H_6, C_6H_6

Reaction (2.1) is a generic reaction that can be used to describe the pyrolysis process and its products(2.1) [22]:

$$\mathrm{C}_n\mathrm{H}_m\mathrm{O}_p(\text{ biomass }) \xrightarrow{\text{heat}} \sum_{\text{liquid}} \mathrm{C}_x\mathrm{H}_y\mathrm{O}_z + \sum_{\text{gas}} \mathrm{C}_a\mathrm{H}_b\mathrm{O}_c + \mathrm{H}_2\mathrm{O} + C\ (\text{char}) \qquad (2.1)$$

The product composition is dependent on the biomass composition and the physical conditions of the process, such as temperature, heating rate, and residence time [13]. The moister content of biomass plays an important role as well [27].

During pyrolysis, the organic materials in the biomass substrate begin to break down at around 350-550°C, and the break down can proceed with the absence of oxygen until 700-800°C [27]. Thereby, the smaller molecules result in the formation of the oils, gases, and solid char [14]. From a chemical aspect, biomass is mainly composed of large, complex polymetric, organic molecular chains such as cellulose, hemicellulose, and lignin [14]. The individual components are subjected to pyrolysis differently, thus varying yield contributions. E.g., cellulose and hemicellulose are the major sources of volatiles and yield condensable gases. Hemicellulose yields more non-condensable gases and less tar than released by cellulose. Lignin degrades slowly, making a major contribution to the char yield [29] [22]. As shown in Figure 2.1, if the wood is completely pyrolyzed, the moister is completely removed at around 160°C, hemicellulose decomposes at 200-300°C, cellulose decomposes in the range of 300-400°C, while lignin decomposition takes place from 280 to 500°C [8] [30].

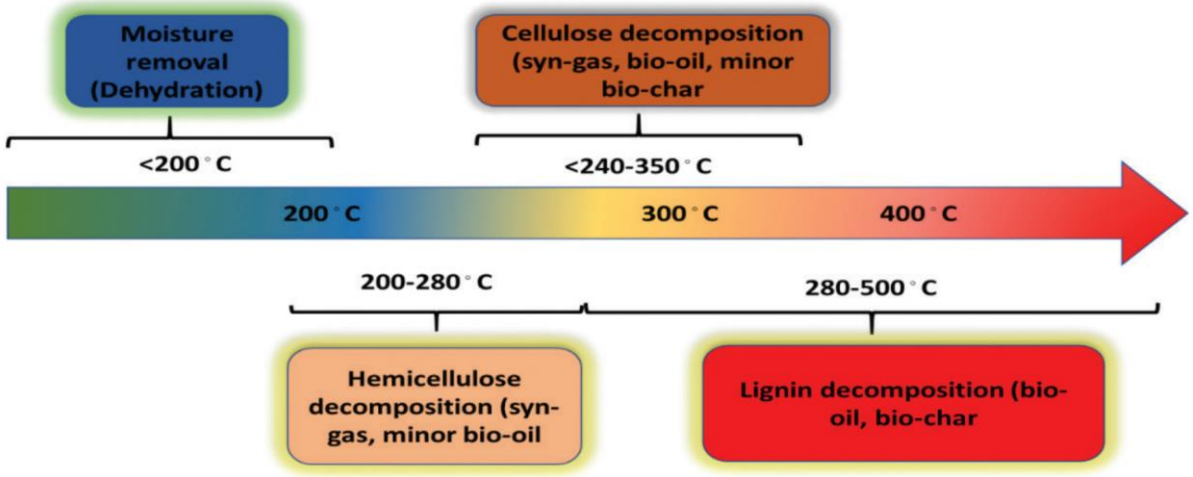

Figure 2.1 Thermal decomposition of biomass (wood) and the products at different temperatures [27].

From a thermal aspect, the pyrolysis reaction mechanisms are complex and generally divided into four (simplified) stages: drying, initial, intermediate, and final stage. The initial stage takes place at around 100-300°C, where the exothermic dehydration of the biomass occurs with the release of water and low-molecular-weight gases such as CO and CO_2 [31]. The third stage is primary pyrolysis taking place in the temperature range of 200-600°C. Most of the vapor or precursor to bio-oil is generated at this stage. The final stage of pyrolysis includes secondary cracking of tar and volatiles into non-condensable gases, which takes place in the temperature range of 300-900°C [22]. Figure 2.2 illustrates the product yield from the decomposition of biomass at different temperatures, conducted by Jahirul et al. [32].

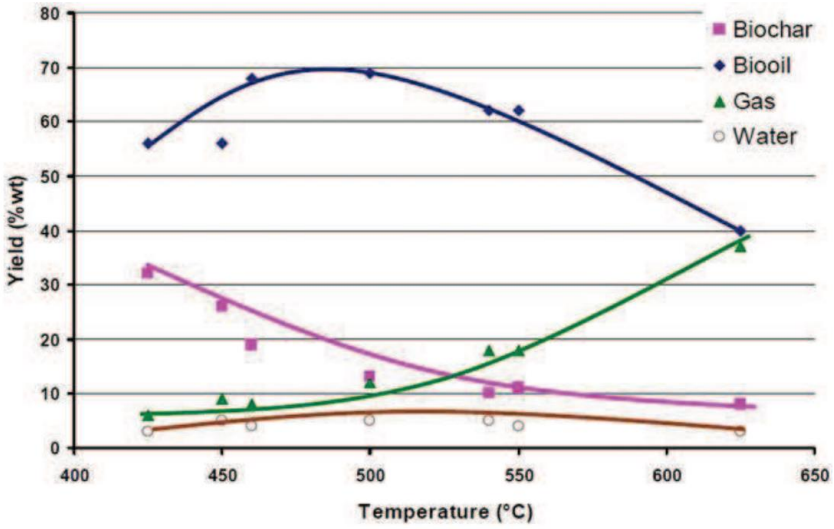

Figure 2.2 Product yield from pyrolysis of biomass as a function of temperature [32].

The actual reaction scheme for wood pyrolysis is extremely complex due to the formation of hundreds of intermediate products. Cellulose is the major component of wood and pyrolyzes over a wide range of temperatures. Thereby, several researchers have been studying cellulose pyrolysis in detail [25], Koufopanos et al. [33] proposed a pyrolysis scheme reaction model illustrated in Figure 2.3.

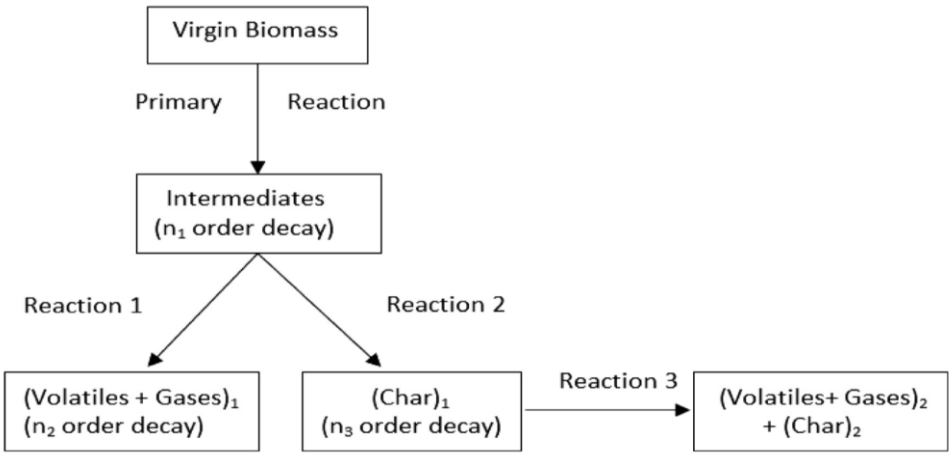

Figure 2.3 Two-step reaction scheme proposed by Koufopanos et al. [33].

This mechanism indicates that biomass decomposes via two parallel reactions to produce volatiles and char. The primary products may further react with char to produce additional volatiles and char with different compositions [34]. The kinetic equations for the scheme mechanism expressed in Figure 2.3 are introduced as follows [25]: Equation (2.2) represents the rate of change in the wood weight fraction. Further, the equations (2.3) and (2.5) are the rate of change in the weight fractions of gases. Finally, equations (2.4) and (2.6) are the rate of change in the char weight fractions.

$$\frac{dm_W}{dt} = -k_1 m_W^{n1} - k_2 m_W^{n1} \tag{2.2}$$

$$\frac{dm_{G1}}{dt} = k_1 m_W^{n1} - k_2\, m_{G1}^{n2}\, m_{C1}^{n3} \tag{2.3}$$

$$\frac{dm_{C1}}{dt} = k_2 m_W^{n1} - k_3\, m_{G1}^{n2}\, m_{C1}^{n3} \tag{2.4}$$

$$\frac{dm_{G2}}{dt} = k_3\, m_{G1}^{n2}\, m_{C1}^{n3} \tag{2.5}$$

$$\frac{dm_{C2}}{dt} = \delta\, k_3\, m_{G1}^{n2}\, m_{C1}^{n3} \tag{2.6}$$

Where m_W is the mass concentration of wood, m_{G1} and m_{G2} are the mass concentrations of primary and secondary gas. m_{C1} and m_{C2} are the mass concentrations of primary and secondary char where n_1, n_2, and n_3 are the orders of the three reactions. k_1, k_2, and k_3 are the rate constants, t is the time, and δ is the yield ratio of secondary char to gas [25] [34].

2.2.1 Pyrolysis oil

The liquid or bio-oil produced from the pyrolysis of biomass is a dark brown, smoky smell and a free-flowing organic liquid mixture [31]. Bio-oil is produced by simultaneous depolymerization and fragmentation of cellulose, hemicellulose, and lignin [22]. Bio-oil is mainly composed of oxygen-containing organic compounds resulting in high thermal instability and low heating values [6]. Bio-oil generally contains a great amount of water (15 – 30 wt%) and hundreds of different organic compounds such as acids, alcohols, phenols, sugars, alkenes, nitrogen, oxygen, and solid particles [6] [21]. The high water content in bio-oil lowers the heating values and makes the phase separation more difficult [27]. Table 2.3 presents typical properties of pyrolysis bio-oil compared to heavy fuel oil.

Table 2.3 Comparison between bio-oil produced from pyrolysis of wood and heavy fuel oil [6] [35] [13].

Physical properties	Bio-oil	Heavy fuel oil
Moisture content (wt.%)	15.0 – 30.0	0.1
pH	2.5	Neutral
Specific gravity	1.2	0.94
HHV (MJ/kg)	16 – 19	40
Density at 15°C (kg/m^3)	1200	890
Viscosity at 500°C (cP)	40 – 100	180
Pour point (°C)	-33	-18
Solids (wt.%)	0.2 – 1.0	1.0
Elemental composition (wt.%)		
C	54 – 58	85
H	5.5 – 7.0	11
O	35 – 40	1.0
N	0 – 0.2	0.3
Ash	0 – 0.2	0.1

The liquid yield from pyrolysis of biomass is normally between 50% - 75% by weight and varies depending on the relative amount of cellulose and lignin in the biomass. Higher cellulose content increases the liquid yields, and high lignin content such as found in bark decreases the liquid yields [35]. Laura et al. [36] performed a fluidized bed pyrolysis experiment of wood pellets and solid recovered fuel (SRF) pellets, with temperatures ranging from 600 - 800°C. The optimum bio-oil yield obtained was 25 and 38 wt.%, respectively at the temperature of 600°C, for both feedstocks.

2.2.2 Pyrolysis biochar

Char is the carbonaceous solid product of biomass pyrolysis, obtained from partial or complete degradation of biomass components [21]. Biochar has a porous structure and is characterized by high surface area and high nutrient retention ability [13] The physical end chemical properties of char are depending on the biomass composition and the pyrolysis operational conditions [21]. Pyrolysis of wood-based biomass usually produces coarser biochar, while crop residues and manures produce more fragile arranged biochar [27]. The calorific value of chars derived from wood-based biomass is about 33 MJ/kg which is relatively high compared to chars derived from MSW and tires, which have a calorific value of about 19 MJ/kg and 29 MJ/kg respectively [14]. The ash content within the char is also an important parameter, as a

higher ash content reduces the heating value of the char as a fuel. Wood-based biochar has very low ash content, typically less than 2% [14].

Usually, pyrolysis of biomass yields 25 – 35% biochar at a temperature between 350°C and 500°C [19]. The elemental composition of biochar is mainly carbon ranging from 53 % to 96 % by weight and can contain oxygen and hydrogen as well [22] [6]. Fagbemi et al. [37] conducted a pyrolysis experiment on wood material with a temperature range of 400 to 900°C. The char yield decreased with increasing temperature. The maximum char yield was 31% achieved at the temperature of 400°C. the HHVs of the char produced were in the range of 33-34 MJ/kg.

Biochar contains a variety of plant nutrients such as magnesium, sulfur, sodium, and manganese, making it useful as a soil enhancement. The nutrient content in biochar can be improved by increasing the pyrolysis temperature. In addition, biochar can be used for co-firing in power stations and can help to reduce ambient carbon emissions by soil carbon sequestration [21].

2.2.3 Pyrolysis gases

Non-condensable pyrolysis gases are produced from the primary decomposition of biomass and secondary cracking of vapors at higher temperatures. Thus, the total product yield of gas is a mixture of primary and secondary gases [22]. As the temperature increases, secondary reactions such as decarboxylation, deoxygenation, dehydrogenation, and cracking take place which further increases the pyrolysis gas yield [27]. The pyrolysis product gas has typically a lower heating value (LHV) in the range of 11-20 MJ/Nm^3, depending on the composition [21].

The non-condensable gas mixture contains CO_2, CO, H_2, and light-hydrocarbons such as CH_4, C_2H_4, C_2H_6 [38]. The decomposition and reforming of carbonyl and carboxyl groups are the primary sources of CO_2 and CO [6]. The lighter hydrocarbons are formed due to the restructuring and breaking of heavier hydrocarbons and tar in the vapor stage [27]. H_2 is produced from the reforming and decomposition of hydrocarbons at higher temperatures [39].

The major reactions for the formation and consumption of CO_2, CO, H_2, and C_2H_6 during pyrolysis of biomass includes the following reactions [40]:

The water-gas reaction (2.7) is an important reaction, describing the reaction of C and H_2O released from biomass to produce H_2 and CO. The reaction is endothermic and requires heat to proceed in its forward direction [41].

$$\mathrm{C} + \mathrm{H_2O} \leftrightarrow \mathrm{CO} + \mathrm{H_2} \qquad \Delta H = +131\ \mathrm{kJ/mol} \tag{2.7}$$

The Boudouard reaction (2.8) where solid carbon (char) reacts with CO_2 to form CO, is the main reaction for reducing CO_2 emissions [42]. The reaction is highly endothermic and thermodynamically favorable at temperatures above 700°C [43]. The CO generated from the Boudouard reaction offers a chemical pathway to produce H_2 by the water gas shift reaction (2.12) [42].

$$\mathrm{CO_2} + \mathrm{C} \leftrightarrow 2\mathrm{CO} \qquad \Delta H = +172\ \mathrm{kJ/mol} \tag{2.8}$$

The dry reforming of methane reaction (2.9) introduces the reaction between CO_2 and CH_4 to produce CO and H_2. The reaction is favored at higher temperatures above 650°C and typically

occurs simultaneously with the reverse water gas shift reaction (2.12) [44]. The dry reforming of methane has been widely studied due to its ability on greenhouse gas reduction and biogas production [45].

$$CO_2 + CH_4 \leftrightarrow 2CO + 2H_2 \qquad \Delta H = +247\ \text{kJ/mol} \tag{2.9}$$

The steam methane reforming reaction (2.10) involves the reaction of CH_4 and H_2O to form CO and H_2. Steam methane reforming of natural gas is the main commercial process for H_2 production and usually proceeds in the presence of a catalyst such as nickel or rhodium. The reaction is strongly endothermic and usually takes place at high temperatures [46].

$$CH_4 + H_2O \leftrightarrow CO + 3H_2 \qquad \Delta H = +206\ \text{kJ/mol} \tag{2.10}$$

Methanation or hydro-gasification reaction (2.11) involves the reaction of C with H_2 producing CH_4. The reaction is relatively slow and favored at higher pressures [19].

$$C + 2H_2 \leftrightarrow CH_4 \qquad \Delta H = -75\ \text{kJ/mol} \tag{2.11}$$

The water-gas shift reaction (2.12) provides the reaction of CO with steam producing CO_2 and H_2. The reaction is moderately exothermic, reversible, thermodynamically favorable at low temperatures 210 - 450°C, and unaffected by pressure changes [47] [48]. The water-gas shift reaction is usually catalyzed by a variety of metallic-based catalysts [49]. The reaction is commonly used in industrial processes such as Hydrogen and ammonia production technologies [50].

$$CO + H_2O \leftrightarrow CO_2 + H_2 \qquad \Delta H = -41\ \text{kJ/mol} \tag{2.12}$$

The gas composition from pyrolysis of biomass is influenced by several factors, including reactor type, heating rate, residence time, reaction medium, biomass particle size, and temperature. The pyrolysis temperature is the most influential factor in most cases [36]. Biomass compositions are also critical in defining the product gas composition, where lignin is the main source for the formation of H_2 and CH_4, hemicellulose contributes to the highest CO_2 emission, and cellulose is responsible for the highest CO emission [51]. Several studies have been conducted to investigate the gas composition from pyrolysis of different biomass feedstocks. Adela et al. [51] studied the gas composition of nine hybrid and nonhybrid grass composts. The gas composition was determined at 700°C. The results are shown in Figure 2.4. The mixture of clover composts (MC) gave the highest H_2 yield (62.17 vol%) and lowest CO and CH_4 formation (12.74 vol%) and (5.10 vol%) respectively [51].

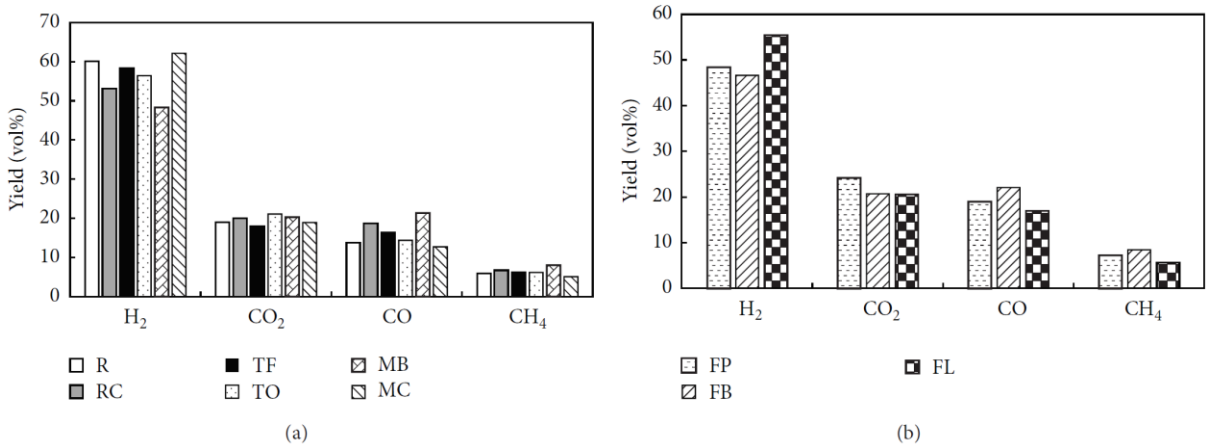

Figure 2.4 Pyrolysis gas composition from pyrolysis of (a) nonhybrid grass composts and (b) hybrid grass composts at temperature 700°C, conducted by Adela et al. [51].

Laura et al. and Fagbemi et al [36] [37] studied the effect of pyrolysis temperature on the product gas yields and gas composition. Some results from these experiments are shown in Table 2.4.

Table 2.4 Product yields and gas compositions from pyrolysis of wood, wood pellets, and straw, with the temperature range of 400-900°C [36] [37].

		Product yield (wt.%)			**Gas composition (vol.%)**				
Feedstock	Temperature (°C)	Tar	Char	Gas	CO	CO_2	H_2	CH_4	C_2H_x
Wood	400	21	33	19	34.2	51.9	1.3	9.3	3.3
	500	33	25	15	39.7	36.6	7.6	12.8	3.3
	600	30	23	21	42.5	23.0	10.8	16.5	7.2
	700	19	22	34	44.3	16.7	15.5	16.1	7.4
	800	12	21	45	50.2	9.1	20.8	14.2	5.8
	900	9	22	48	53.5	5.0	25.3	12.1	4.1
Wood pellets	600	28	22	50	47	15	14.5	16	7.5
	700	16	19	65	43	18	17	16	6
	800	5	18	77	37	21	23	14	5
Straw	700	15	33	34	41	15.8	19.2	15.3	8.7
	800	10	31	43	48.1	8.4	23.4	13.7	6.5
	900	7	30	51	53.3	4.5	24.6	12.1	5.5

As shown in Table 2.4, and by comparing the gas product yields and gas compositions from pyrolysis of wood, wood pellets, and straw, wood pellets resulted in the highest gas product yield (77wt.%) achieved at 800°C. All cases show an increase in gas product yield and H_2 production as the temperature increases. Pyrolysis of wood pellets and straw gave the highest H_2 formations of 23% and 23.4% by volume respectively, achieved at 800°C. The CH_4 production was highest at approximately 700°C and declined afterward in all three cases.

2.3 Effect of operational conditions on biomass pyrolysis products

Depending on the operational conditions, mainly temperature and heating rate, pyrolysis is categorized as slow, intermediate, fast, and flash pyrolysis. Slow pyrolysis is defined as a carbonization process operating at low heating rates, long residence time, and low temperatures. The main product from this process is charcoal [27] [30]. Intermediate pyrolysis is characterized by a lower heating rate compared to fast pyrolysis. Accordingly, less tar is generated due to more controlled chemical reactions take place [19]. Fast or flash pyrolysis is characterized by high heating rates and high temperatures, where the main goal is to maximize the production of liquid or bio-oil [12]. Table 2.5 summarizes the impact of operational conditions on the product yield from different modes of pyrolysis of wood.

Table 2.5 Typical feedstock requirements, operational conditions, and product yield of different modes of pyrolysis (dry-wood basis) [23] [13] [19].

	Feedstock	**Operational conditions**			**Product yield**		
	Particle size	Temperature (°C)	Heating rate °C/min	Residence time	Solid (%)	Liquid (%)	Gas (%)
Slow pyrolysis	Moderate-large	300-500	<10	Minutes to days	35	30	35
Intermediate pyrolysis	Small-large	400-500	300	Minutes	25	50	25
Fast pyrolysis	Small (<1 mm)	400-650	1-1000	0.5-5 s	12	75	13
Flash pyrolysis	105-250 µm	650-1300	>1000	<1 s	<20	<70	<20

2.3.1 Pyrolysis temperature

The pyrolysis temperature has a significant effect on the product distribution and properties. The gas components released during the pyrolysis of biomass vary with different temperatures. Figure 2.5 shows the behavior of different gas components released from the pyrolysis of wood as a function of temperature [22].

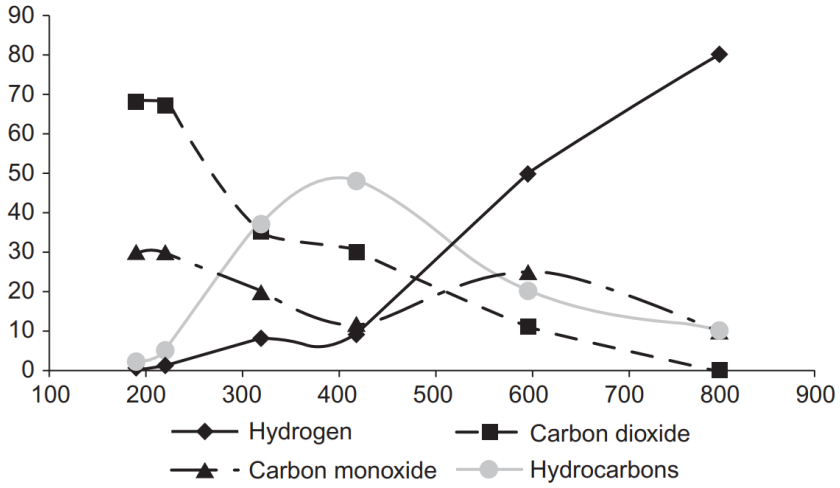

Figure 2.5 Release of gases (vol.%) during pyrolysis of wood as a function of temperature [22].

The amount of char produced is also affected by the pyrolysis temperature. Low temperatures increase the char while high temperatures decrease the char produced. Encinar et al. studied the effect of temperature on char and gas production from grape bagasse pyrolysis. He reported that the heating value of char increases with the temperature as shown in Figure 2.6. This is due to the increase of fixed carbon content in the char as the temperature is increased. The amount of non-condensable gases, such as CO_2, CO, H_2, and CH_4, increases with the temperature [22].

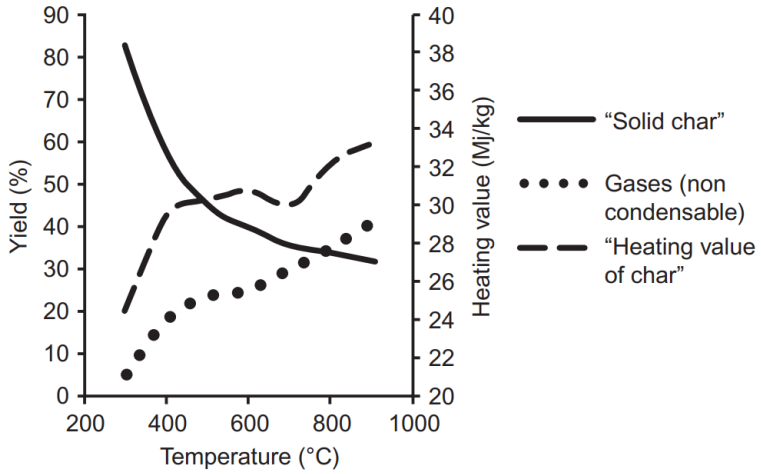

Figure 2.6 Char and gas yield from pyrolysis of grape bagasse as a function of temperature reported from Encinar et al. [22].

The liquid yield from pyrolysis of lignocellulosic biomass is also influenced by the pyrolysis temperature. Usually, the liquid yields attain their highest yield at temperatures between 400 and 550°C. When the temperature is increased above 600°C, the liquid and char products are transformed into gases because of the dominant secondary cracking reactions [21].

Rover et al. studied the effect of temperature on bio-oil produced from pyrolysis of red oak wood. He reported a maximum char yield of 31.1wt.% at temperature 350°C, a maximum bio-

oil yield of 66.7wt% at 400°C, and the highest non-condensable gas yield of 26.3wt.% at 550°C [6]. Demirbas (2007) studied the effect of temperature on the yield of char and liquid from pyrolysis of hazelnut shell, beechwood, spruce wood, and organics of MSW. He reported that char yield decreases as the temperature increases. The HHV of char from biomass samples increases as the pyrolysis temperature increases. The highest liquid yields from the biomass samples were achieved at temperatures ranging between 380°C and 530°C. The experimental results conducted by Demirabs (2007) are illustrated in Figure 2.7 and Figure 2.8 [52].

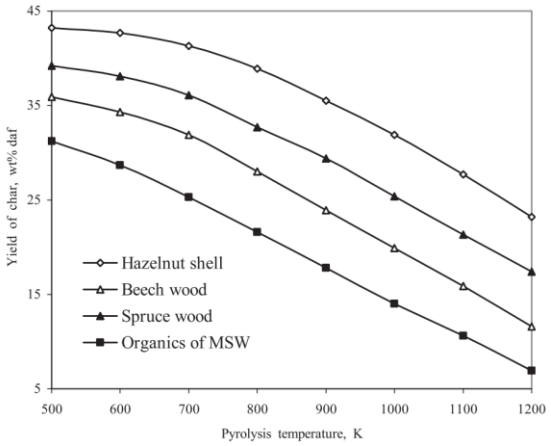

Figure 2.7 Effect of temperature on char yield [52].

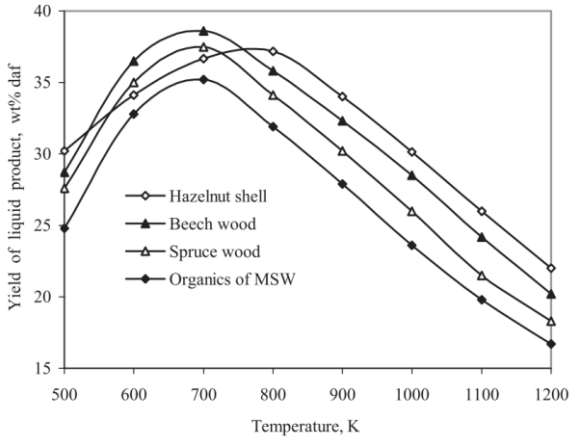

Figure 2.8 Effect of temperature on liquid yield [52].

2.3.2 Heating rate

The heating rate of biomass pyrolysis has a fundamental influence on the product yield and composition. At fast heating rates, biomass is subjected to quick fragmentation, resulting in more gases and lower char yield. Fast heating rates also improve bio-oil production because mass and heat transfer is increased, and secondary reactions have less time to occur. Accordingly, slow heating rates produce more char [22] [21]. In addition, high heating rates contribute to increasing the yield of CO and CO_2, decrease the water content in the liquid product and reduce the pore volume in the char [6].

The operational conditions, including the heating rate, can be modified to satisfy the requirements of the desired end products. To maximize char production, slow heating rate and low final temperature are recommended. For maximation of the liquid yield, a high heating rate, moderate final temperature (450-600°C), and a short gas residence time are preferred. To maximize the gas yield, moderate to slow heating rate, high temperature (700-900°C), and a long gas residence time is required [52] [22].

Harding et al. [53] studied the effect of heating rate for the pyrolysis of sawdust on the liquid yield. They observed that the oil yield increased by increasing the heating rate. As shown in Figure 2.9, the bio-oil increases significantly when the heating rate is increased from 500 to 700 °C/min, whereas there is no marked change of oil yield when the heating rate is increased from 700 to 1000 °C/min.

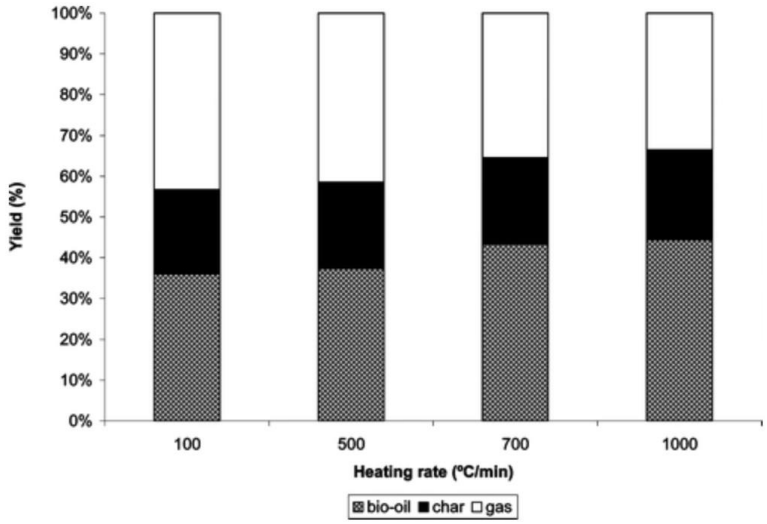

Figure 2.9 Product yield from pyrolysis of sawdust as a function of heating rate, at a pyrolysis temperature of 500°C, reported from Harding et al. [53].

Chen et al. [54] performed slow pyrolysis experiments of bamboo biomass and investigated the effect of heating rate on the pyrolysis product yield. An increase in the heating rate resulted in to decrease in the char and bio-oil yield and an increase in the gas yield, as illustrated in Figure 2.10.

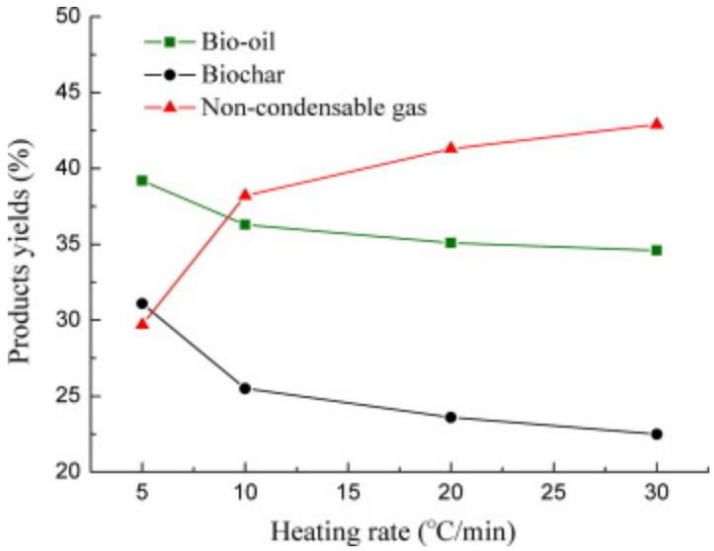

Figure 2.10 Product yield from pyrolysis of bamboo as a function of heating rate, at a temperature of 700°C, reported from Chen et al. [54].

2.3.3 Particle size

The pyrolysis product yield can be influenced by the particle size and shape of the biomass due to its impact on the heating rate. In finer biomass particles, the condensable gases have an easier path to escape before secondary cracking occurs. As a result, the liquid yield increases. In contrast, larger biomass particles contribute to increasing the char yield [22]. Smaller particles,

in general, enable heat and mass transfer to obtain uniform temperatures within the biomass particles during pyrolysis. The liquid production is improved by minimizing the secondary vapor cracking [21].

Zaman et al. [55] studied the effect of particle size of palm kernel shell on pyrolysis product yield. They used a series of particle sizes ranging between 0.35 and 2 mm and pyrolysis temperature ranging between 380 and 600°C. As shown in Figure 2.11 and Figure 2.12, the highest liquid yield was obtained at a particle size of 0.35 mm and temperature 450°C. The highest char yield was obtained from the largest particle size (1-2 mm).

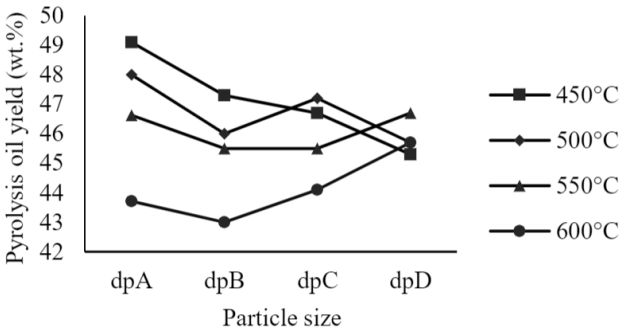

Figure 2.11 Effect of particle size on liquid yield, reported from Zama et al. [55].

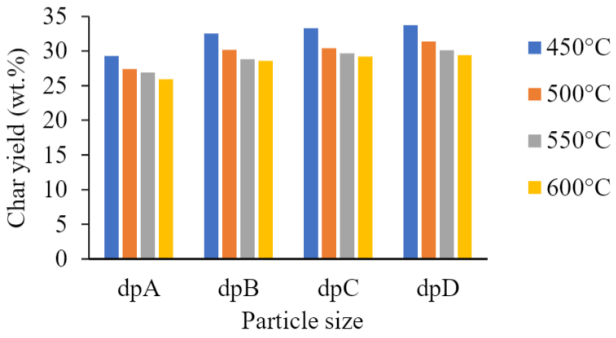

Figure 2.12 Effect of particle size on char yield, reported from Zaman et al. [55].

2.3.4 Pretreatment of biomass

Biomass feedstock usually needs pretreatment before pyrolysis. The purpose of the pretreatment is to enhance the pyrolysis efficiency and improve the desired product yields. Pretreatment technologies include milling/grinding, torrefaction, drying and densification/pelletization [22] [21]. Milling or grinding biomass into smaller particles is a common procedure due to easier feeding into the reactors and improve pyrolysis efficiency.

Drying of biomass before pyrolysis increases the energy efficiency of the process [21]. Because a kilogram of water in biomass needs 2.26 MJ to vaporize and therefore, high moisture content results in a substantial energy loss [31]. Lignocellulosic biomass such as wood usually has a moisture content of 30 to 60% and can be as high as 90% for some types of biomass [22]. For the pyrolysis process, drying of biomass to a moisture content of 10-15% is usually required [31]. Some research reported the effect of dried biomass on product yields. It improves the quality of generated syngas by lowering the CO_2 content and increasing the H_2 and CH_2 contents. Others also verified a lower liquid yield generated from pyrolysis of dried biomass [21].

Densification or pelletization of biomass by applying mechanical force produces biomass pellets which usually take the shape of small cylinders. Densified biomass is characterized by easier handling, reduces storage and transportation costs, high volumetric energy density, lower moisture contents, and higher bio-oil yields from pyrolysis [31] [21] [6].

2.4 Pyrolysis reactor

A pyrolysis reactor is the major component of any pyrolysis process. The choice and design of a pyrolysis reactor are dependent on satisfying specific conditions within heating temperature, heating rates, and vapor product residence time [27]. Thus, different types of pyrolysis reactors have been developed, including fixed beds, fluidized beds, heated kiln, rotating cone, ablative, screw feeder, and vacuum reactors [38]. The reactor designs differ mainly in the way the feedstocks are fed through the reactor and the mechanism of heat transfer [23]. Figure 2.13 illustrates some of the heating methods related to pyrolysis reactors [6]. The heat transfers to the reactors could be gas-solid or solid-solid. In gas-solid, the heat is transferred from the hot gas to the biomass particles through convection. In solid-solid, the heat is transferred from the reactor wall to the biomass particles through conduction [32].

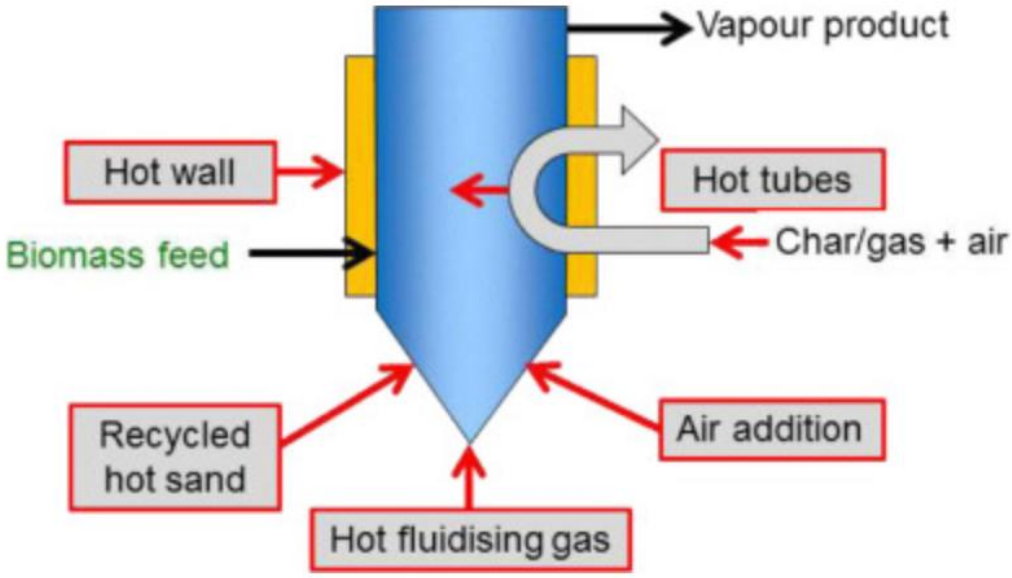

Figure 2.13 Heat transfer methods in pyrolysis reactors [6].

Table 2.6 summarizes the characteristics and the status of common pyrolysis reactors.

Table 2.6 Characteristics and status of common pyrolysis reactor units [6].

Reactor type	Status	Bio-oil yield (wt.%)	Complexity	Feed size specification	Inert gas need	Specific reactor size	Scale-up	Gas quality
Fluidized bed	Commercial	75	Medium	High	High	Medium	Easy	Low
CFB and transported bed	Commercial	75	High	High	High	Medium	Easy	Low
Rotating cone	Demonstration	70	High	High	Low	Small	Medium	High
Entrained bed	Laboratory	60	Medium	High	High	Medium	Easy	Low
Ablative	Laboratory	75	High	Low	Low	Small	Hard	High
Screw or auger	Pilot	60	Medium	Medium	Low	Small	Medium	High
Vacuum	None	60	High	Low	Low	Large	Hard	Medium

3 Gasification of biomass

There are three types of reactors or gasifiers used for biomass gasification: fixed or moving bed, fluidized bed, and entrained flow gasifiers. They differ mainly in their flow conditions, gas-sild contact mode, and residence time of biomass inside the reactors [56] [57].

This chapter includes the basic principles of biomass gasification. Among the gasification reactor types, fluidized bed gasification reactor will only be discussed in this chapter due to its relation to the study. A literature study on the simulation of the biomass gasification process is also introduced.

3.1 Principles of biomass gasification

Biomass gasification processes, in contrast to pyrolysis, tend to maximize the conversion of biomass feedstock into valuable gases [19]. The product gas mixture is called synthesis gas or syngas, which consists of CO_2, CO, CH_4, H_2, H_2O, and small amounts of light and heavier hydrocarbons [56]. In addition, and contrast to pyrolysis, gasification requires a gasifying medium such as steam, air, or oxygen to rearrange the molecular structure of the biomass to produce gases [22]. Biomass particles undergo a chain of conversion processes, which includes drying, pyrolysis, combustion, and char gasification [58] [22]. Figure 3.1 illustrates the main conversion steps that occur during biomass gasification.

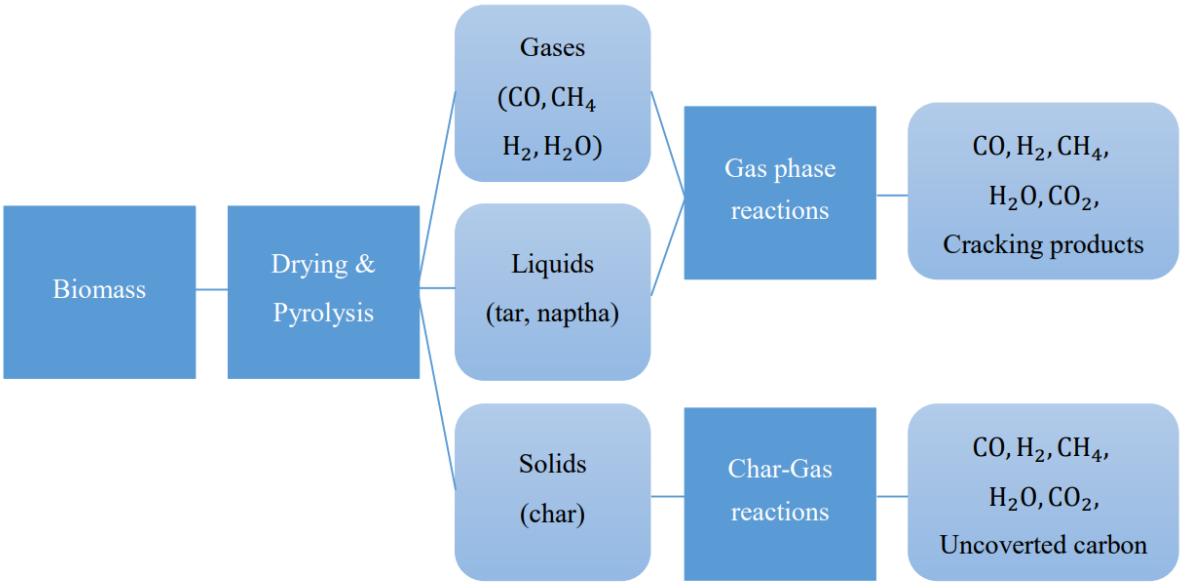

Figure 3.1 Main conversion processes in biomass gasification [58].

Typical reactions involved in the biomass gasification process are the oxidation reactions presented by partial oxidation reaction (3.1), oxidation of carbon reaction (3.2), hydrogen combustion reaction (3.3), and carbon monoxide combustion (3.4) in addition to the previously mentioned reactions listed from (2.7) to (2.12) in chapter 2.2.3 [51] [22].

$$2C + O_2 \leftrightarrow 2CO \qquad \Delta H = -222\ \mathrm{kJ/mol} \qquad (3.1)$$

$$C + O_2 \leftrightarrow CO_2 \qquad \Delta H = -394\ \text{kJ/mol} \qquad (3.2)$$

$$H_2 + 1/2O_2 \leftrightarrow H_2O \qquad \Delta H = -242\ \text{kJ/mol} \qquad (3.3)$$

$$CO + 1/2O_2 \rightarrow CO_2 \qquad \Delta H = -283\ \text{kJ/mol} \qquad (3.4)$$

These oxidation reactions are exothermic. The main product of the oxidation step is the thermal energy needed for the gasification process, while the gas produced is a mixture of CO, CO_2, and H_2O [56].

3.2 Fluidized bed gasification reactor

Fluidized bed gasification reactors are characterized by effective temperature distribution and high mass and heat transfer rates compared to other reactor types [19]. The bed material (e.g., sand) inside the reactor act as a heat carrier and a mixing enhancer. The biomass is typically fed from the top or sides and gets mixed relatively quickly over the entire fluid bed's regime [22]. The syngas yield is typically high, while the tar content is low due to the secondary cracking reactions under high temperatures [13]. The fluidized bed gasification reactors are classified into two types: bubbling fluidized beds and circulating fluidized beds. They differ mainly in fluidized gas velocity and gas path [59]. Figure 3.2 shows the main characteristics of fluidized bed gasification reactors.

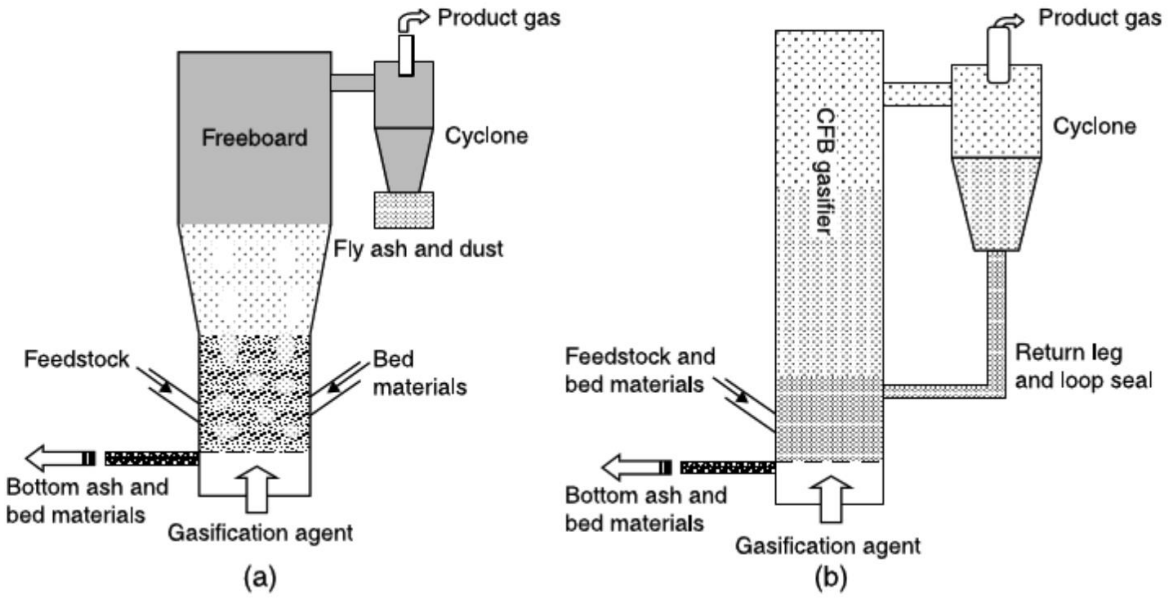

Figure 3.2 Scheme of fluidized bed gasification reactors: (a) bubbling and (b) circulating fluidized bed [19].

3.3 Simulation of biomass gasification

Process simulation is a useful method for simulating flows in complicated systems such as chemical reactors. In general, process simulation provides information about how an existing system will respond when the operational conditions are varied [60].

Many simulation software and models used for the simulation of biomass gasification processes have been developed. Aspen Plus is a popular software for simulating coal conversion and has been used for simulating biomass gasification processes. The software includes an extensive library of physical property models and unit operation models, as well as quick and accurate process simulation functions, and an advanced measurement method [61]. Niko et al. developed a model for biomass gasification in an atmospheric fluidized bed gasifier using the Aspen Plus simulator. The model was used to predict performance such as product gas composition of a laboratory scale biomass gasifier. The model gave reasonable results compared to the experimental results [62].

Computational fluid dynamics (CFD) software and models are commonly used for the simulation of biomass gasification processes. Among such software are Ansys Fluent, Ansys CFX, OpenFoam, and Barracuda (CPFD) software. CFD software is characterized by giving the ability to study the flow behavior inside the reactor and testing the flow and fluid effects on surfaces [63]. In general, all CFD models for multiphase flow can be divided into two categories: Eulerian-Eulerian and Eulerian-Lagrangian approaches. Both particle and fluid phases are treated as interpenetrating continua in the Eulerian-Eulerian approach. This solution has been used to simulate the fluidization processes for many years, as it can estimate and predict the microscopic characteristics of a process with remarkably low computational cost. The Eulerian-Eulerian method has difficulty modeling flows with a variety of particle types and sizes, this is due unrecognition of the discrete character of the particle phase. These difficulties can be avoided by using the Eulerian-Lagrangian method. The Eulerian-Lagrangian model treats the gas as continuous and particle as discrete phase [64]. This model uses the Navier Stokes equations with an appropriate averaging method to model the fluid phase [65]. The Eulerian-Lagrangian approach works effectively for both dune and dense multiphase flows. However, the computation time grows in proportion to the number of parcels simulated. This means, the denser the flow is, the longer it takes to compute. The disadvantage of using this model is the high computational costs. This is mainly because a high number of parcels is needed for the statistical mean values of the dispersed phase. The grid generation for complex geometries requires the usage of the multiblock concept. As a result, every new parcel placement needs a long and complex search method, which is highly time-consuming [66].

The Computational Fluid Particle Dynamic (CPFD) method for solving particle-laden fluid flows is used in Barracuda Virtual Reactor (VR) software. Barracuda VR is specialized CFD software that is commonly used for simulation and analysis of fluidized bed reactors and other gas-solid processes [67]. The software can predict performance when changing the unit operational conditions, geometry, inlets and outlets, flow rates, and particle properties [60]. The Barracuda VR software uses the multiphase particle-in-cell (MP-PIC) model. This numerical approach solves the fluid phase with the Eulerian computational grid and models the solid phase with Lagrangian computational particles [68]. A given number of particles having the same properties are expressed by parcels to minimize the computational costs [60]. The present thesis uses Barracuda VR software for the simulation of the biomass gasification process.

4 Pyrolysis experiments

The pyrolysis experiments were performed at the University of South-Eastern Norway, department Porsgrunn. The overall aim is to build and construct the pyrolysis reactor unit and perform pyrolysis experiments. Furthermore, study the pyrolysis product yields and the product gas compositions. This chapter presents the pyrolysis experimental setup and procedure along with feedstock analyses.

4.1 Pyrolysis feedstock

Wood pellets manufactured by Felleskjøpet were used as the feedstock for the pyrolysis experiments. The pellets consist of 100% wood having a diameter of 6 mm and a length range between 5 – 30 mm. Figure 4.1 shows the size distribution of the wood pellets.

Figure 4.1 Wood pellets as received.

The higher heating value (HHV), ultimate and proximate analysis presented in Table 4.1 were carried out by Eurofins Environmental Testing Norway AS, using the following standard test methods: Solid recovered fuels method SS-EN 15407 for determination of carbon, nitrogen, and hydrogen contents, SS-EN ISO 18123 for the volatile matter, EN-ISO 18122 for the ash, and SS-EN 15400 for the higher heating values. The fixed carbon content was calculated by difference. The analyses received from the source are attached in Appendix B.

Table 4.1 Ultimate and proximate analysis of wood pellets.

	Ultimate analysis (wt.%)[a,b]					**Proximate analysis (wt.%)[a]**				
Biomass	C	H	N	O[c]	S	Moisture[d]	Volatile matter [a]	Ash[a]	Fixed carbon[a,c]	HHV (MJ/kg)
Wood pellets	51.3	6.1	0.1	42	0.01	7.9	83.9	0.55	15.55	18.774

a = dry basis, b = ash-free, c = by difference, d = as received

4.2 Experimental set-up

A tubular reactor is designed and constructed to perform a set of pyrolysis experiments. Figure 4.2 and Figure 4.3 show the designed and constructed pyrolysis reactor. The reactor is cylindrical shaped made of steel with a diameter of 50 mm and length of 200 mm. The reactor consists of two sections, section A and B. Section A is fixed inside the furnace and has three inlets and outlets, one for biomass feeding, one for nitrogen flushing, and one for product gas outlet. Section B is made of aluminum and used as a biomass feeder, which is tightly inserted into section A through the wall gasket.

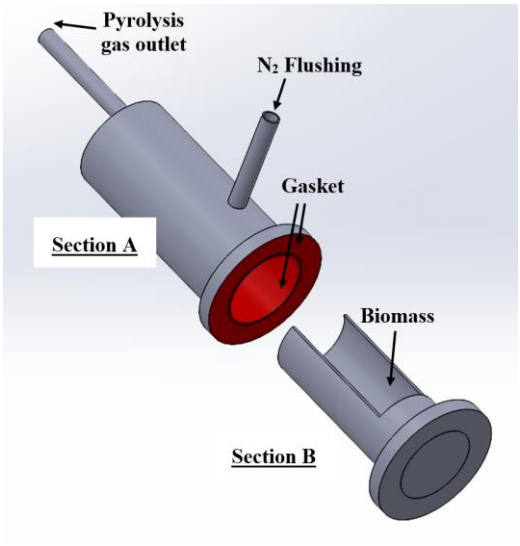

Figure 4.2 Pyrolysis reactor design.

Figure 4.3 Front view of constructed reactor.

The constructed reactor is inserted horizontally into a muffle furnace of type Nabertherm model L15/11/B410 programmer and chimney, having a maximum allowable temperature of 1100°C. The furnace temperature is shown on the integrated display and can be adjusted to the desired temperature. Figure 4.4 illustrates a schematic diagram of the pyrolysis process.

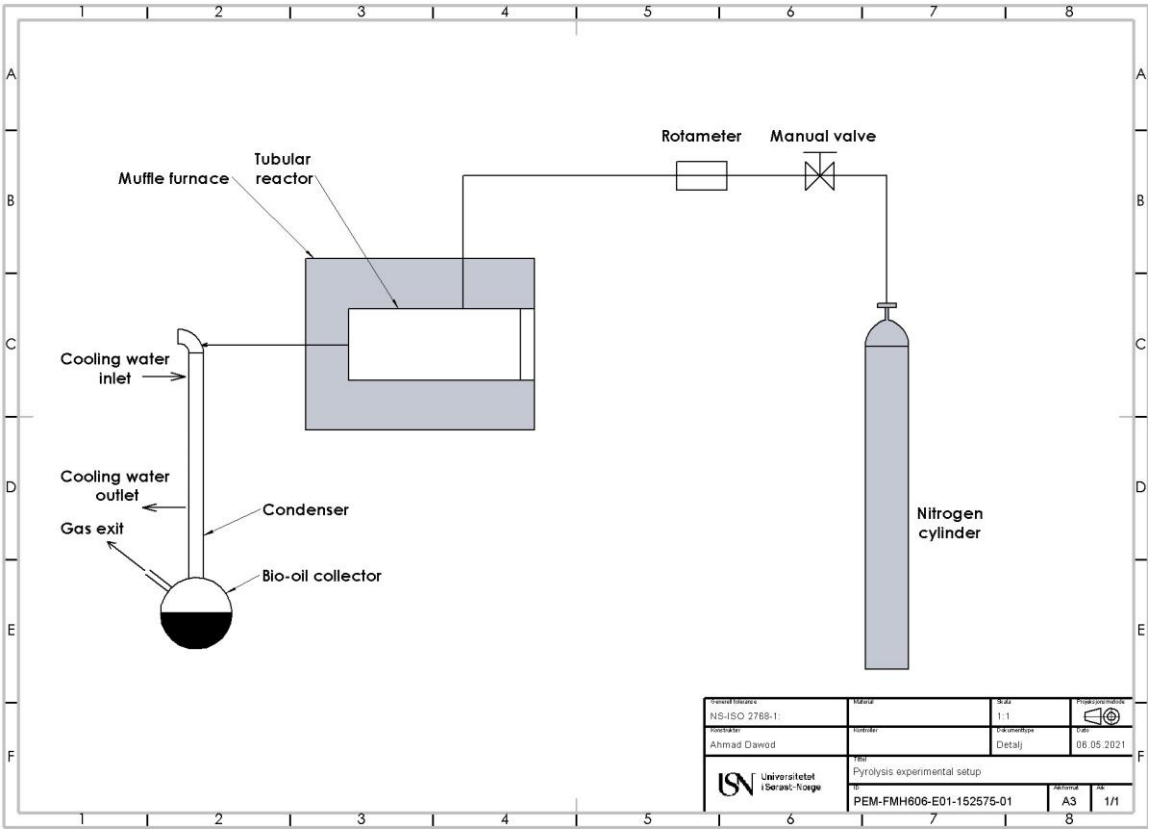

Figure 4.4 Schematic diagram of the biomass pyrolysis process.

The schematic diagram is drawn using the SolidWorks software. Nitrogen is used as a carrier gas to avoid any oxygen to flow into the system. The nitrogen flow is supplied from a gas cylinder, controlled by a gas cylinder, and measured with a rotameter. The reactor is connected to a water-cooled condenser to collect the condensable vapors. Pyrolysis liquid yield is collected in a bio-oil collector. A gas chromatograph (GC) SRI 8610C using helium as a carrier gas, is used to determine the gas composition fraction (O_2, N_2, CH_4, CO_2, and CO). The GC is located in the experimental facility and uses a thermal conductivity detector (TCD). Helium does not measure H_2 accurately at lower concentrations. This is mainly because helium and H_2 have a close relation in weight. Therefore, the H_2 composition was calculated by difference. Gas-tight syringes with shut-off valves were used for gas sampling. Figure 4.5 and Figure 4.6 show the gas chromatograph (GC) and the water-cooled condenser used for experiments.

Figure 4.5 SRI 8610C gas chromatograph.

Figure 4.6 Water-cooled condenser.

4.3 Experimental procedure

Pyrolysis experiments were performed in the pyrolysis reactor using a temperature of 500°C. The furnace was firstly programmed to 20°C above the desired temperature. Using 20°C above the desired temperature was to compensate for the temperature drop during insertion of the samples. The cooling water supply for the condenser was then opened and the furnace switched on. The nitrogen flow supply was opened and adjusted to approximately 0.1 L/min. The carrier gas flow (Helium) for the GC was opened, and the GC was switched on.

A wood pellet sample was then weighted (approximately 50g) and placed in the aluminum capsule. Once the furnace reached 20°C above target temperature, the capsule was inserted into the reactor and the closure flange was closed tightly. The nitrogen flow was then increased to flush out any oxygen inside the reactor. Once the smoke was observed in the condenser, gas samples were extracted in 2 – 3 min intervals using syringes. After the pyrolysis of wood pellets was completed, the nitrogen flow was maintained until the furnace was cooled to 200°C. This was to avoid oxidation of the char. The extracted gas samples were analyzed with the GC.

Isopropyl alcohol (IPA) was used to wash any tar attached to the condenser. The tar content was heated at 105°C by a laboratory furnace to evaporate the solvent within the tar. Finally, the aluminum capsule was taken out and the char weight was measured. The most important safety issues and concerns related to the operation of the pyrolysis unit are listed in Appendix C.

Mass balance:

In all experiments conducted, the initial sample of wood pellets was weighted before each experiment. The solid and liquid yields after complete pyrolysis were weighted separately. By applying material balance to the pyrolysis process, the weight of the produced gas can be calculated using Equation (4.1). Figure 4.7 illustrates the material balance applied to the pyrolysis process.

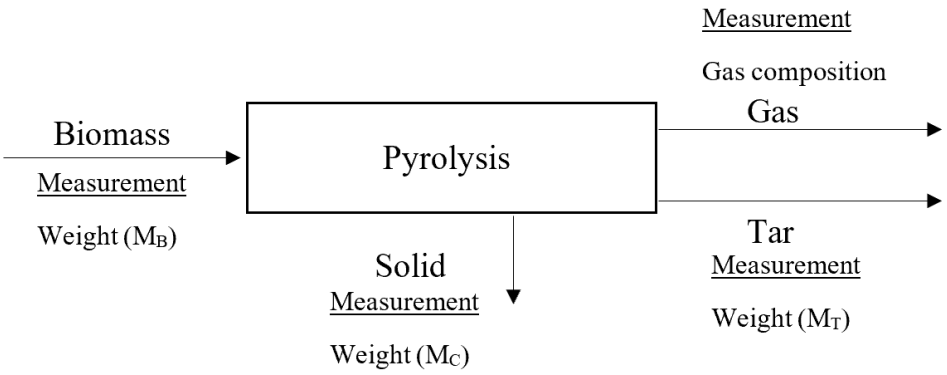

Figure 4.7 Material balance.

$$Mass\ of\ the\ gas\ (\mathrm{M}_G) = \mathrm{M_B} - (\mathrm{M_C} + \mathrm{M_T}) \tag{4.1}$$

The mass fractions of the product yields are calculated using equations (4.2) and (4.3).

$$\text{Liquid yield } = \frac{\mathrm{M_T}}{\mathrm{M}_B} \times 100 \tag{4.2}$$

$$\text{gas yield } = \frac{\mathrm{M}_G}{\mathrm{M}_B} \times 100 \tag{4.3}$$

5 CPFD simulation of biomass gasification

Computational particle fluid dynamic (CPFD) software was used to simulate the biomass gasification reactor. The Barracuda Virtual reactor (VR) version 17.4.1 software simulates multiphase hydrodynamics, heat balance, and chemical reactions of fluid-particle systems in three dimensions. The Lagrange approach is used for the particle phase, and the Eulerian approach is used for the gas phase. Pyrolysis data obtained from different studies were used as an input for the simulation.

The aim was to study the composition of the synthesis gas obtained from gasification of wood pellets and compare them with the experimental results performed at USN and conducted by (Bandara, 2021, P.44) [65]. Further, to study the effect of pyrolysis gas composition and reactor temperature on the synthesis gas composition. This chapter discusses the simulation setup and procedure used in Barracuda software to establish the simulation model.

5.1 Mesh and geometry

For simulation of the biomass gasification reactor, a geometry with 8.83 cm square cross-section and 100 cm height was created. The geometry can be constructed using software that handles CAD geometries such as AutoCAD and SolidWorks. Afterward, the geometry was imported to Barracuda as a .STL file and meshed. Figure 5.1 shows the meshed geometry (Grid), the initial bed material and dimension of the geometry, and the locations of transient data points.

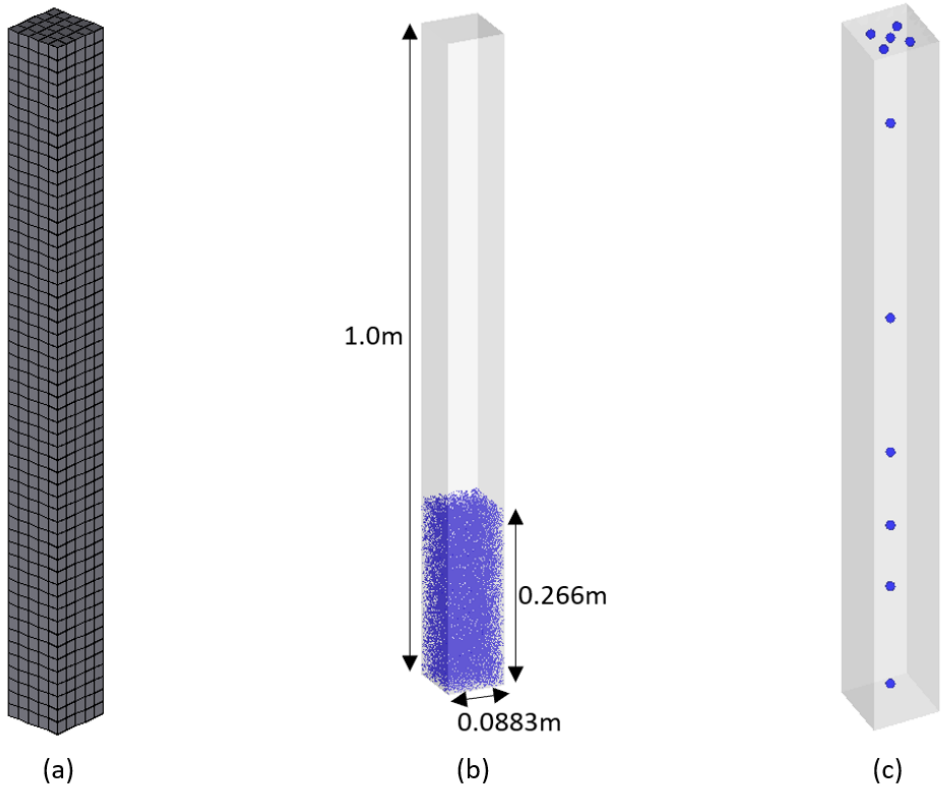

Figure 5.1 Simulation set-up: (a) Meshed geometry (b) Initial bed material and geometry dimensions (c) Transient data points.

The simulated grid was generated with 6000 cells in total. Sand (SiO_2) particles with a mean diameter of 300 microns and density of 2650 kg/m^3 were used as bed material. The bed material was initially at 0.266 m height as illustrated in Figure 5.1b depicted with blue color. The transient data points (sensors) located at the center along the column are to measure the temperature and the pressure at different locations of the reactor. The transient data points located at the top surface of the reactor measures the gas composition. The location of the transient data points is shown in Figure 5.1c depicted with blue dots.

It should be noted that the simulation was done using a square-sectioned geometry to avoid small and missing grid sections that can arise in a cylindrical-shaped geometry. According to the study done by (Bandara, 2021, P.44) [65], at least one biomass particle should be able to fit within the cell to avoid computational errors. However, the geometry has the same cross-section area as the cylindrical geometry used in experiments.

5.2 Initial and boundary conditions

The boundary conditions within the reactor were specified as shown in Figure 5.2a. Air was used as the gasification agent. The top of the reactor was set as a pressure boundary. The flow boundary conditions were specified as air and biomass inlet. The air inlet was set up at the bottom of the reactor while the biomass inlet was located at 0.254 m above the bottom plane. Figure 5.2b shows the thermal boundary condition. Thermal boundary condition was specified to cover the entire reactor which represents the controlled wall temperature.

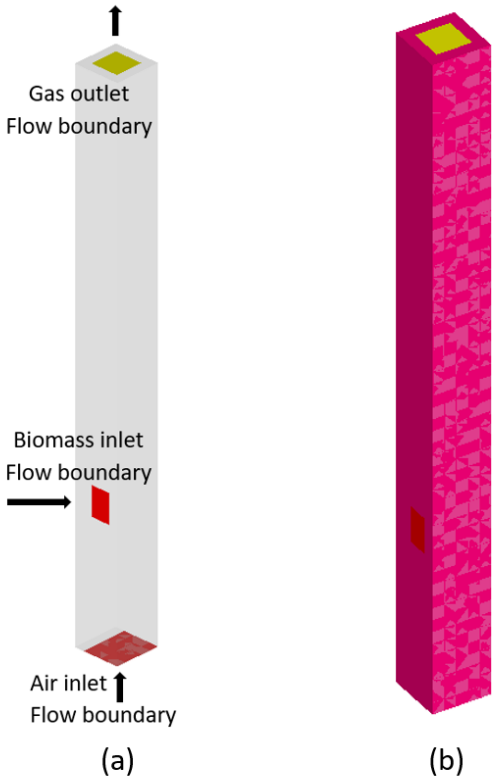

Figure 5.2 Boundary conditions: (a) Flow boundaries (b) Thermal boundary.

The initial conditions for the gasification reactor were also defined. The reactor was initially filled with pure nitrogen at 1 atm and the temperature was varied according to the simulated case. The bed material is initially 100% sand (SiO_2) with a particle volume fraction of 0.6. The starting temperature was specified to be similar to the target operational temperature for all simulated cases.

5.3 Input data

There are several drag models available in Barracuda. Wen-Yu/Ergun was adopted for the simulation because prior simulations done at USN used the Wen-Yu/Ergun drag model and the results showed a good match to the experimental data [69]. Table 2.1 shows the specified biomass properties, inlet flows, and simulation parameters used in the simulation.

Table 5.1 Biomass particle properties, inlet flows, and simulation parameters used in the simulation.

Biomass properties	
Type	Wood pellets (spherical shaped)
Size	2 mm
Inlet temperature	27°C (300K)
Density	1000 kg/m^3
Char density (after pyrolysis)	300 kg/m^3
Inlet flows	
Air	3 kg/h
Biomass	2.4 kg/h
Biomass carrier gas (N_2)	0.5 L/min
Air-Fuel ratio	1.25
Simulation parameters	
Close-pack volume fraction	0.6
Maximum momentum redirection from collision	40%
Normal-to-wall momentum retention coefficient	0.85
Tangent-to-wall momentum retention coefficient	0.85
Diffuse bounce	3
Drag model	Wen-Yu/Ergun

Several chemical reactions might occur in an air gasification reactor. The considered reactions for the simulation are previously mentioned and are as follows: The water-gas reaction (2.7), boudouard reaction (2.8), steam methane reforming reaction (2.10), water gas shift reaction (2.12), char partial oxidation reaction (3.1), hydrogen combustion (3.3) and carbon monoxide combustion reaction (3.4). The kinetic rates relevant to these reactions were also included in the simulation. The chemical kinetics included in this study were taken from the Ph.D. thesis done by (Bandara, 2021, P.44) [65]. Figure 5.3 shows the reaction rates included under the rate coefficient data input.

Chemistry Rate Coefficients Manager

ID	Name	Reaction Type	Coefficient Type	Expression	Comment
00	k0	Volume-Average	Arrhenius Chem Rate	6.4e+09 e^(-39260 / T)	water gas shift reaction
01	k1	Volume-Average	Arrhenius Chem Rate	0.029 e^(-4094 / T)	WGSR equlilibrium
02	k2	Volume-Average	Arrhenius Chem Rate	4.78e+08 e^(-8046 / T)	CO combustion
03	k3	Volume-Average	Arrhenius Chem Rate	2.2e+09 e^(-13110 / T)	H2 combustion
04	k4	Volume-Average	Arrhenius Chem Rate	2.8e+09 e^(-24400 / T)	CH4 combustion 4.2
05	k5	Volume-Average	Arrhenius Chem Rate	4.4e+11 e^(-15150 / T)	CH4 combustion 4.3
06	k6	Volume-Average	Arrhenius Chem Rate	6.14e+13 e^(-28116 / T)	CH4 reforming equlibrium
07	k7	Volume-Average	Arrhenius Chem Rate	3e+08 e^(-15000 / T)	CH4 reforming
08	k8	Volume-Average	Arrhenius Chem Rate	147000 e^(-13590 / T)	Char oxidation 6.1
09	k9	Volume-Average	Arrhenius Chem Rate	1040 T^1 e^(-11200 / T)	steam gasification
10	k10	Volume-Average	Arrhenius Chem Rate	3.42 T^1 e^(-15600 / T)	CO2 gasification
11	k11	Volume-Average	Arrhenius Chem Rate	4.4e+08 e^(-26400 / T)	tar reforming
12	k12	Volume-Average	Arrhenius Chem Rate	1.58e+15 e^(-24300 / T)	tar oxidation

Figure 5.3 Reaction rates for the gasification reactions.

5.4 Simulation procedure

The simulated biomass was wood pellets. To define the wood pellets in the simulation software, the fraction of the volatiles and solid must be clarified. From the proximate analysis Table 4.1, wood pellets are broken into 83.9 wt.% volatiles, 15.55 wt.% fixed carbon, 0.55 wt.% ash, and 7.9 wt.% moisture in the pyrolysis stage. The amount of ash is very small; thus, the ash content was neglected. The moisture content was included in the volatile phase. Biomass char is considered to consist of pure carbon.

Experimental data conducted from other studies were used and fitted into the Barracuda simulation software. The product gas composition from pyrolysis of wood pellets, conducted from other studies, is listed in Table 2.4. Product gas composition includes CO, CO_2, H_2, CH_4, and H_2O gases. The Barracuda software requires to specify the volatiles in mass percentages. Therefore, the volume percentage of the gases was converted into a mass percentage using equation (5.1). The ideal gas assumption was adopted. Thereby, the molar fraction is the same as the volume fraction.

$$Mass\ fraction = \frac{Volume\ fraction * Molecular\ weight}{Total\ weight} \tag{5.1}$$

Three simulation cases were established by changing the reactor temperature and fitting the pyrolysis gas compositions according to data from the literature. The specific data for each case are tabulated in Table 5.2.

Table 5.2 Input data for the simulation cases.

Case number	**Temperature (°C)**	**Volatiles (wt.%)**	**Char (wt.%)**	**Gas composition (wt.%)**					
				H_2O	H_2	CH_4	CO_2	CO	Tar (benzene)
Case-A	800	85	15	9	2	12	36	41	
Case-B	800	85	15	9	1	11	24	37	18
Case-C	900	85	15	9	2	12	36	41	

For Case-A, the reactor temperature was set to 800°C and the pyrolysis gas composition for 800°C was fitted. Case-B was modified by setting the reactor temperature to 800°C and fitting the pyrolysis gas composition for 700°C. It was assumed that if the mixing is not complete at the feeding point, the temperature can drop down to 700°C. In this case, the composition of tar (benzene) was included because pyrolysis yields more liquid at lower temperatures. Case-C is modified by increasing the reactor temperature up to 900°C and use the gas compositions for 800°C. The special aim of these cases was to study the effect of temperature and pyrolysis gas composition on biomass gasification. And thereby, compare the results with the experimental results from other studies done at the USN gasification rig.

6 Results and Discussion

This chapter presents the results obtained from pyrolysis of wood pellets experiments, along with a discussion of the results. The results were further compared to other pyrolysis experiments obtained from the literature. Similarly, the results from the three simulated cases are presented and compared with experimental data.

6.1 Pyrolysis experiments

The pyrolysis experimental rig is a newly built unit, hence there were some modifications and operational problems during the experiments. Due to technical reasons, it was only possible to get good results from only one of the pyrolysis experiments. Among the operational problems experienced during this study are the leakages from closing flanges. Whereas the gas could not pass through the solvent in the impingements bottles due to the pressure. However, this problem was solved by replacing the impingement bottles with a water-cooled condenser.

The pyrolysis experiment was performed with a reactor temperature of 500°C and the initial sample of wood pellets was weighted to 37.8g. It took approximately 9 minutes to complete the pyrolysis. The char and tar products were weighed, and the product gas percentage was calculated by material balance using Equation (4.1), (4.2), and (4.3). The tar produced has a dark brown appearance. Figure 6.1 shows the end-products obtained from pyrolysis of wood pellets at 500°C.

Figure 6.1 Tar and char produced from pyrolysis of wood pellets at 500°C.

Figure 6.2 shows the product yields obtained from pyrolysis of wood pellets at 500°C. The char, tar, and gas fractions were measured to be 29.2%, 22.5%, and 48.3% by weight, respectively. There is a possibility of escaping some non-condensed tar with the gas. Therefore, the actual tar content may be a little bit higher, and the gas content may be lower.

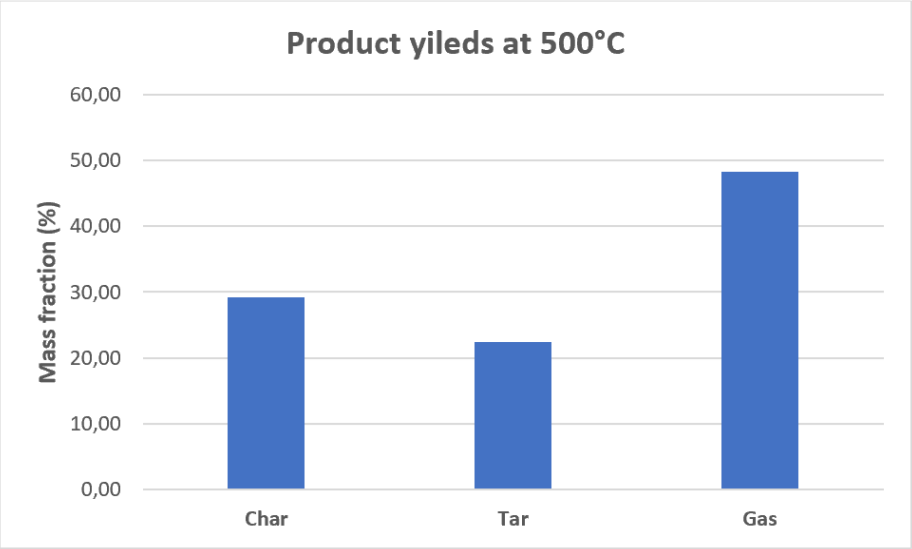

Figure 6.2 Product yields from pyrolysis of wood pellets at 500°C.

There were no studies found on pyrolysis of wood pellets at 500°C. Therefore, it was decided to compare the results with the pyrolysis experiments performed for wood listed in Table 2.4. This is to compare the trend of the product yields and study the validity of the pyrolysis experiment. As both wood pellets and wood are lignocellulosic biomass, the same product trends are expected. Figure 6.3 shows the product yields from the pyrolysis experiment of wood pellets compared to product yields from pyrolysis of wood obtained from the literature. The trend of char yield agreed well with the literature, while the experimental tar yield was lower, and the experimental gas yield was significantly higher. The high gas yield and low tar yield in the experiment might be due to escaping of non-condensed tar with the gas.

Nevertheless, it is expected that pyrolysis of wood pellets will produce less tar than wood. This is because wood pellets have less moisture content compared to wood and according to the literature, less moisture content in the biomass contributes to fewer tar yields.

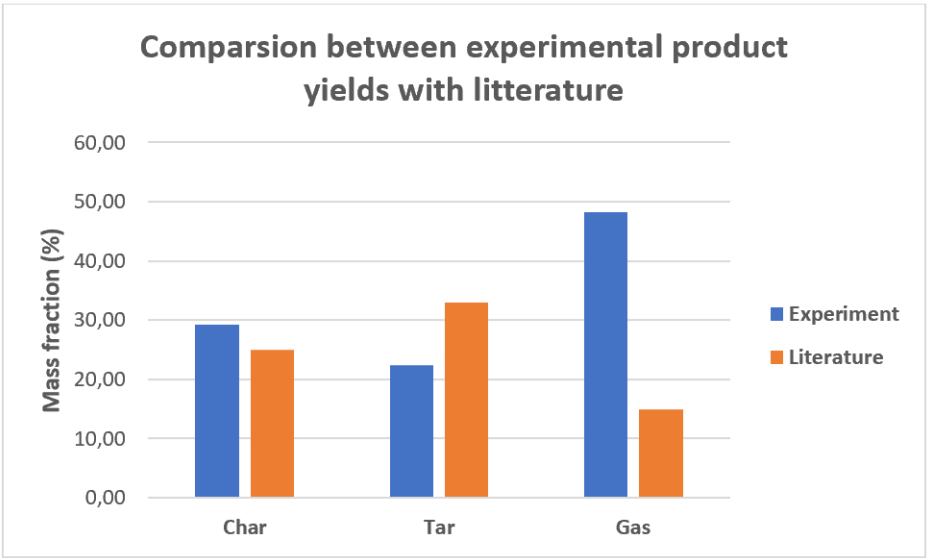

Figure 6.3 Comparison between experimental results and literature results at 500°C.

Once the smoke was observed in the condenser, the gas samples were extracted in 1-2 minutes intervals using syringes. Figure 6.4 and Figure 6.5 show the results for the gas compositions analyzed by the gas chromatographer (GC), measured after 9 minutes of pyrolysis. The rest of the results and graphs obtained from the GC after 2, 4, 7, and 8 minutes of pyrolysis are attached in Appendix D.

The cumulative value of the gas compositions was above 100%, as shown in Figure 6.5. This might be due to other gas components that are not calibrated such as Ethane and hydrogen. Usually, the composition of H_2 is calculated by difference. However, as the gas composition obtained from the GC analysis was above 100%, it was not possible to calculate it. Furthermore, the GC could not differentiate between CO and CH_4 in different peaks. From experience, this is mainly due to high concentrations of CO and CH_4. As shown in Figure 6.4, the GC measured the two gases as CH_4 and in other cases as CO. However, it was observed a shoulder in the analysis, where it starts to differentiate but suddenly decreases. This means that both gases are presented in the product gas. The N_2 presence in the analysis is due to N_2 flushing inside the reactor during the operation.

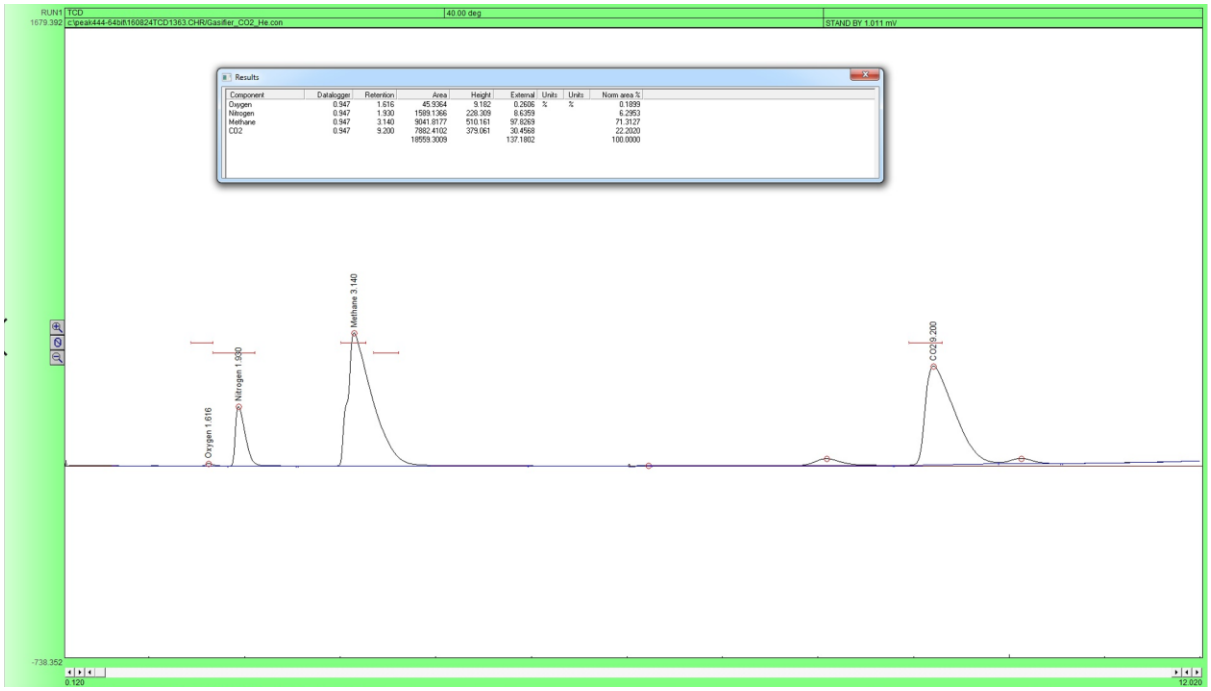

Figure 6.4 Gas analysis from the GC after 9 minutes of pyrolysis.

Component	Datalogger	Retention	Area	Height	External	Units	Units	Norm area %
Oxygen	0.947	1.616	45.9364	9.182	0.2606	%	%	0.1899
Nitrogen	0.947	1.930	1589.1366	228.309	8.6359			6.2953
Methane	0.947	3.140	9041.8177	510.161	97.8269			71.3127
CO2	0.947	9.200	7882.4102	379.061	30.4568			22.2020
			18559.3009		137.1802			100.0000

Figure 6.5 Gas volume fractions from the GC after 9 minutes of pyrolysis.

Due to the mentioned issues, the sum of CO and CH_4 were introduced together. The concentration of H_2 was determined by difference for the case of 2 minutes, as it was the only case with cumulative gas composition below 100%. Figure 6.6 indicates the evolution of the product gas with time at pyrolysis temperature of 500°C. The H_2 concentration was only

analyzed after 2 minutes and was 6.7%. The cumulative CH_2 and CO concentration increased with time and achieved their peak concentration at 9 minutes. The highest concentration of cumulative CH_3 and CO was 97.8%. The concentration of CO_2 increased with time and declined after 7 minutes. The highest concentration of CO_2 was 46.2%.

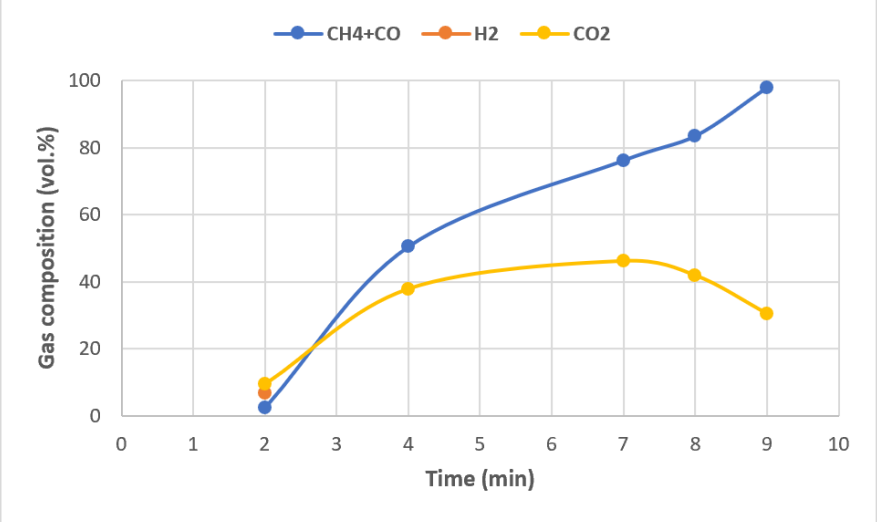

Figure 6.6 Product gas production with time at 500°C.

The gas compositions were averaged and compared to results from pyrolysis of wood at 500°C obtained from the literature. Figure 6.7 shows the average gas composition from the experiment compared to the results listed in Table 2.4. The average concentrations of cumulative CH_2 and CO, H_2, and CO_2 were found to be 62%, 6.7%, and 33.1% respectively. The experiment seems to agree well with the results from the literature, especially for H_2 and CO_2. The Higher concentration of cumulative CH_4 and CO and lower CO_2 concentration might be due to less moisture content within the wood pellets compared to the wood. The steam generated from the moisture content enhances mainly the water gas shift reaction (2.12), which consumes CO and produces more CO_2. Dong et al. [70] and Xiong et al. [71] studied the effect of moisture content of different biomass on the product gas compositions during pyrolysis. Both studies agreed that high moisture content within the biomass contributes to higher CO_2, lower CO, and CH_4, and higher H_2 concentrations in the product gas. This agrees well with the results from the experiment compared to results from the literature.

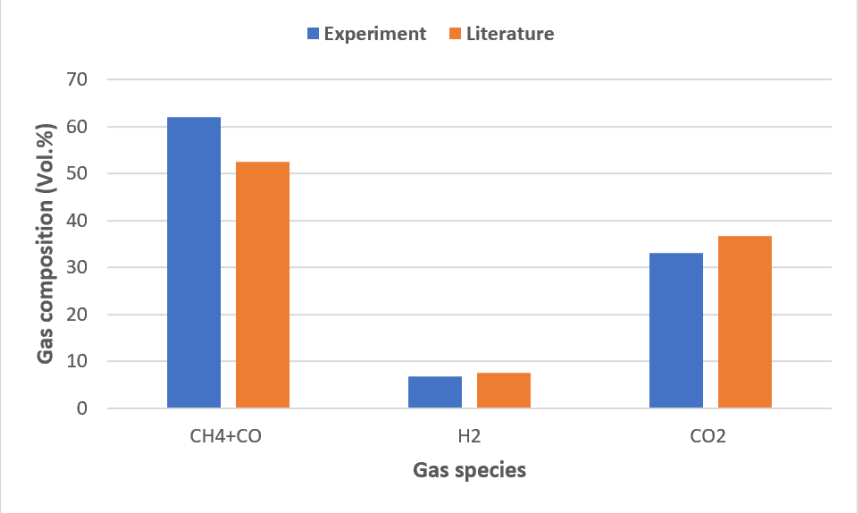

Figure 6.7 Average product gas composition obtained from experiment and literature at 500°C.

However, other factors might have contributed to the variations between experimental and literature results. The type of wood and wood pellets were not identified, whereas different wood types have different biochemical compositions. Uncertainty during the experiment, gas leakages, sampling issues, higher density for the wood pellets might have also influenced the product yields.

6.2 CPFD model

This chapter includes the results of the three simulated cases created for biomass gasification reactor. The influence of the pyrolysis gas composition and reactor temperature on the synthesis gas composition are presented and discussed. The synthesis gas compositions from the simulation were further compared with the experimental data obtained from other studies.

The total simulation time for each case was set to 200 seconds with a time step of 0.001 seconds. The gas compositions measured by the transient data points were averaged for the last simulated 100 seconds.

6.2.1 Case-A

Case-A was modified by setting the reactor temperature to 800°C using the pyrolysis gas composition for 800°C. Figure 6.8 shows the mass fraction of product species at the reactor outlet plotted after 100s of simulated time. The average mass fraction of CO was 10.4%, CO_2 was 39.4%, CH_4 was 4.2% and H_2 was 1.1%.

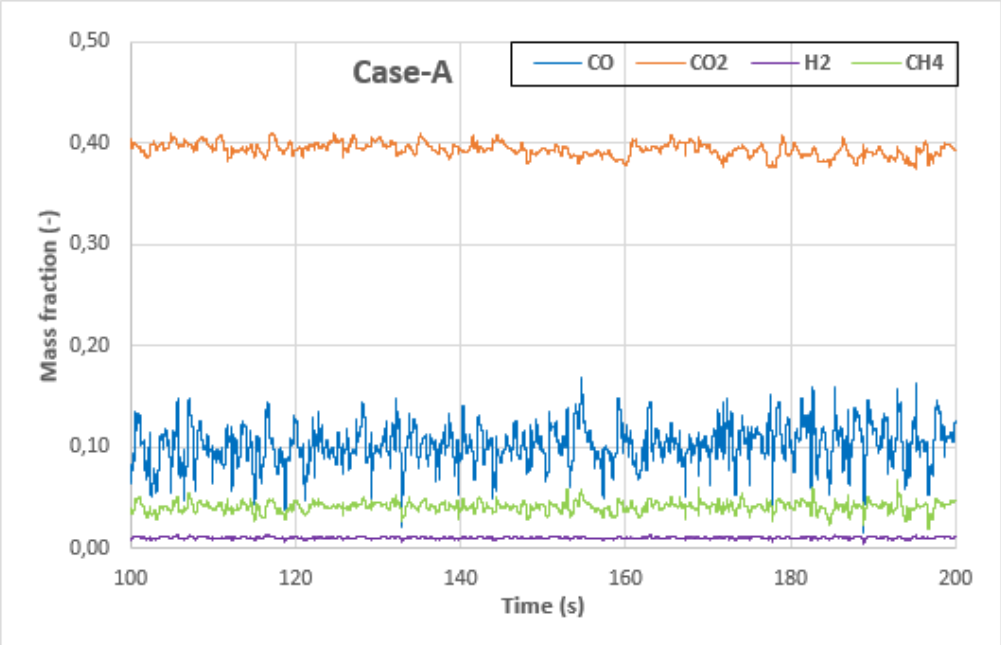

Figure 6.8 Case-A: Outlet mass fraction variation with time.

Figure 6.9 shows an outline of the (a) fluid temperature (b) particle temperature and (c) particle volume fraction along the bed, plotted at 200s. These parameters were only studied for this case. As there are no significant changes within temperature, and the air flow was kept constant, the same behavior for the other cases is assumed. As shown in Figure 6.9, fluid and particle temperatures are above 800°C (1073K), which is the desired temperature. This indicates that the gasification reactions are continuously maintained. From Figure 6.9c, the particles seem to be well mixed, which is good in terms of temperature distribution. The air flow might be a little bit high, but as long the particles remain within the bed it is accepted. However, limited air flows can reduce the generation of combustible gases such as CO, H_2, and CH_4.

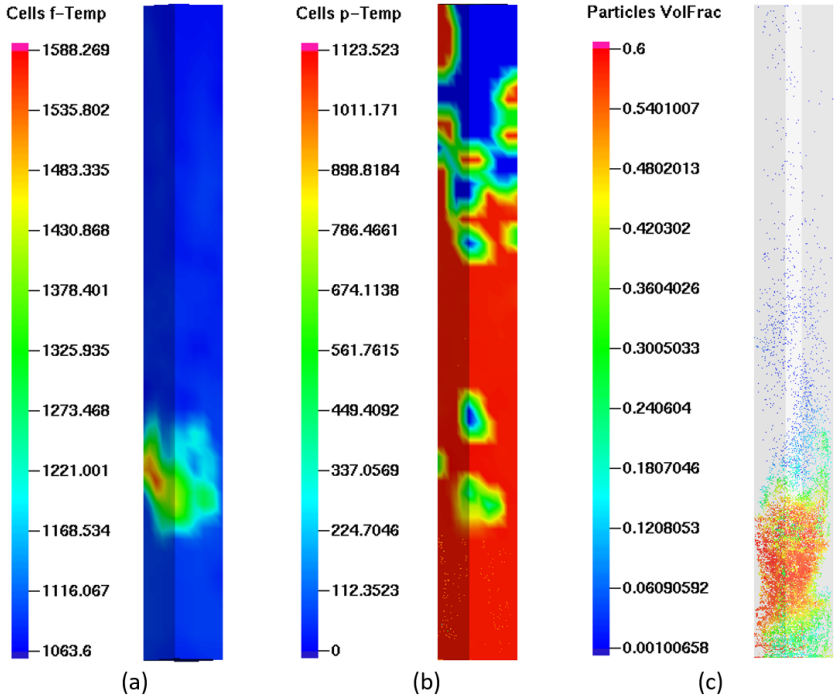

Figure 6.9 Reactor conditions (a) Fluid temperature [K] (b) Particle temperature (c) Particle's volume fraction.

6.2.2 Case-B

In Case-B, the reactor temperature was kept at 800°C and the pyrolysis gas composition for 700°C was fitted. Figure 6.10 shows the mass fraction of product species at the reactor outlet plotted after 100s of simulated time. The average mass fraction of CO was 13.2%, CO_2 was 32.4%, CH_4 was 4.1% and H_2 was 0.9%. As the pyrolysis gas composition for 700°C was fitted in this case, more tar will be produced. Thereby, the tar composition was modified within the volatiles and the tar reactions were included in the simulation.

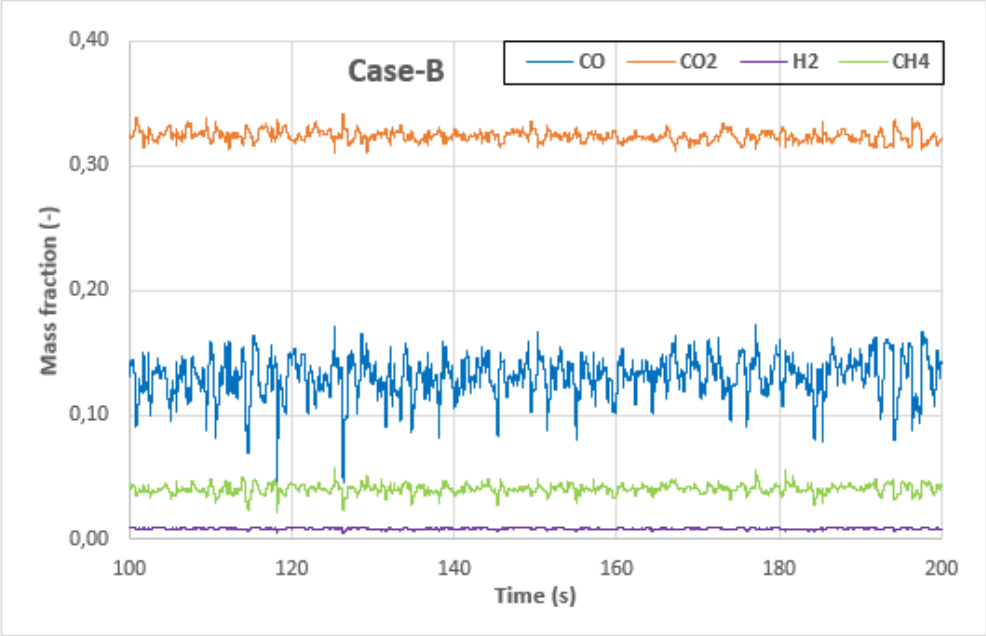

Figure 6.10 Case-B: Outlet mass fraction variation with time.

6.2.3 Case-C

Finally, Case-C was modified by setting the reactor temperature to 900°C and fitting the pyrolysis gas composition for 800°C. Figure 6.11 shows the mass fraction of product species at the reactor outlet plotted after 100s of simulated time. The average mass fraction of CO was 13.1%, CO_2 was 37.9%, CH_4 was 3.9% and H_2 was 1.2%.

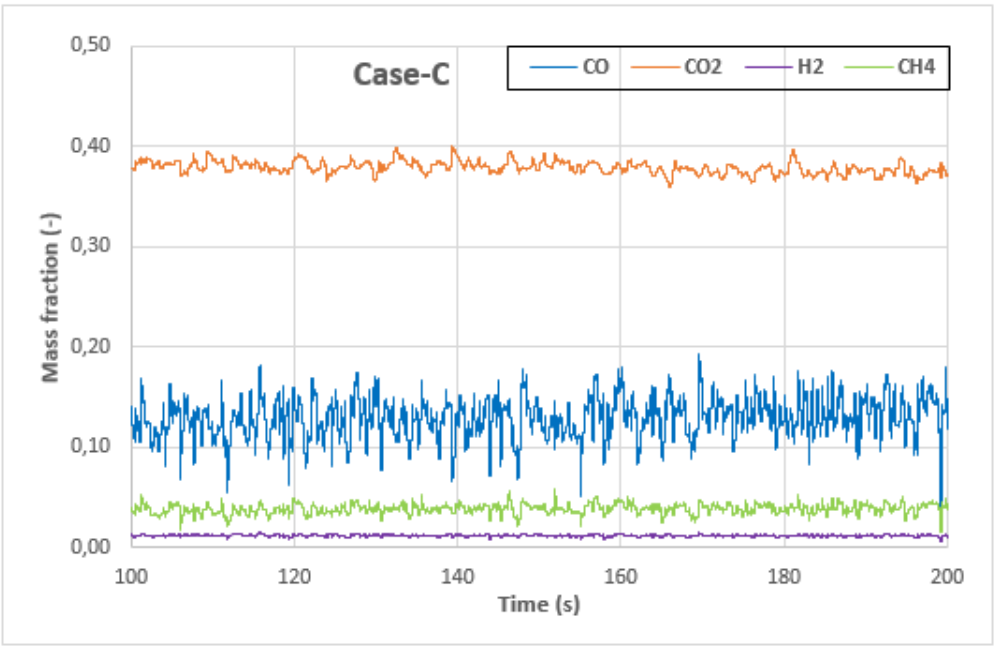

Figure 6.11 Case-C: Outlet mass fraction variation with time.

6.2.4 Comparison

From Figure 6.8, Figure 6.10, and Figure 6.11, the calculated product mass fractions are showing a noisy and unsteady behavior, whereas the steady-state is never reached. This is due to the unsteady characteristics of the fluidized bed, where different chemical and physical transformations taking place. However, it was noticed from the plots that the average mass fractions were stable over time.

The average gas composition from the three cases was converted into a molar basis and is presented in Figure 6.12 and Table 6.1. The percentage of other gases includes N_2, O_2, and H_2O. In addition to these gases, benzene is only included in Case-B. In all cases, N_2 contributed to the highest molar concentration and ranged between 41.5% and 43.5% of the total volume composition. This is reasonable, as nitrogen is an inert gas and does not react with other gases. The molar concentration of O_2 were monitored to be very close to zero. This is mainly due to the occurrence of oxidation reactions. The H_2O molar concentration were measured to be 2.5%, 1.6%, and 1.2% for Case-A, B, and C, respectively. The lower percentage of H_2O produced in Case-C is mainly due to the increase of temperature to 900°C. Where higher temperatures enhance the water gas reaction (2.7) to proceed forward. Which in term produces more H_2. In all cases, the molar concentration of CO_2 was highest, and then comes H_2 and CO, respectively. The lowest produced gas component was CH_4.

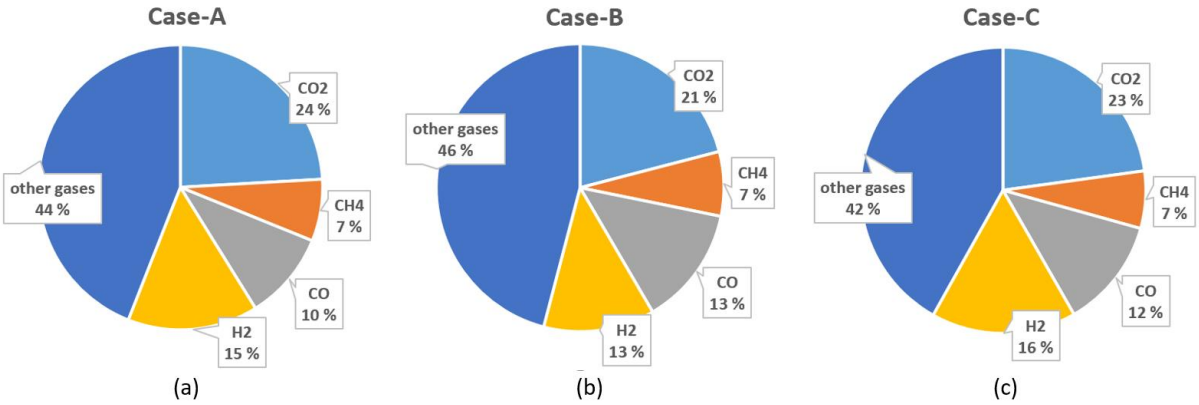

Figure 6.12 Molar compositions of the gas species monitored at the reactor outlet for (a) Case-A (b) Case-B (c) Case-C.

Case-A and Case-B were simulated for the same reactor temperature but different pyrolysis gas compositions, therefore, the results from the two cases are compared with the input pyrolysis gas composition to study the effect of the pyrolysis step. Figure 6.13 and Figure 6.14 show the input pyrolysis gas compositions for Case-A and B respectively, compared to the synthesis gas compositions.

The molar concentration of CO_2 increased slightly by 3% and 2.6% in the synthesis gas for Case-A and B, respectively. In the contrast, the CO concentration decreased significantly by 27% and 29.9% in the synthesis gas for Case-A and B, respectively. The concentration of CH_4 decreased by 6.9% and 7.1% in the synthesis gas for Case-A and B, respectively. The concentration of H_2 decreased by 8.2% and 4.7% in the synthesis gas for Case-A and B, respectively.

The increase of CO_2 is mainly due to the oxidation reactions in the gasifier. The consumption of CO is mainly due to enhance of the CO combustion reaction (3.4) and water gas shift reaction (2.12), where both reactions produce more CO_2. Consumption of methane is mainly due to steam methane reforming reaction (2.10), which in term produces more CO.

It was observed that higher concentrations of the combustible gases including CH_2, CO, and H_2 released in the pyrolysis stage contributed to higher concentrations of these gases in the synthesis gas. This means that the pyrolysis stage is critical in deciding how much CH_4, CO, and H_2 will be produced in the synthesis gas.

From Figure 6.13, Figure 6.14 and according to the mentioned arguments, the pyrolysis gas composition seems to have a significant effect on the synthesis gas compositions, especially on the production of the combustible gases. This is mainly because 85% by weight of the synthesis gas was produced during the pyrolysis of biomass step.

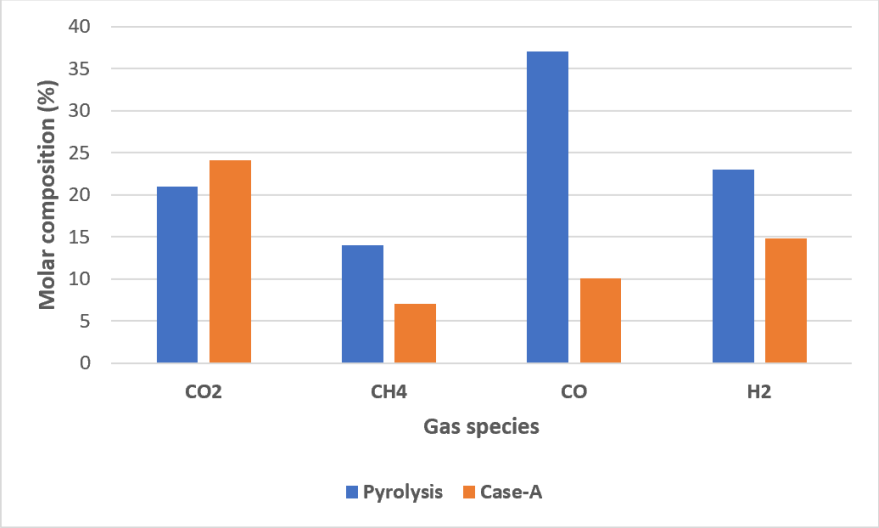

Figure 6.13 Case-A: Input pyrolysis gas composition compared to synthesis gas composition.

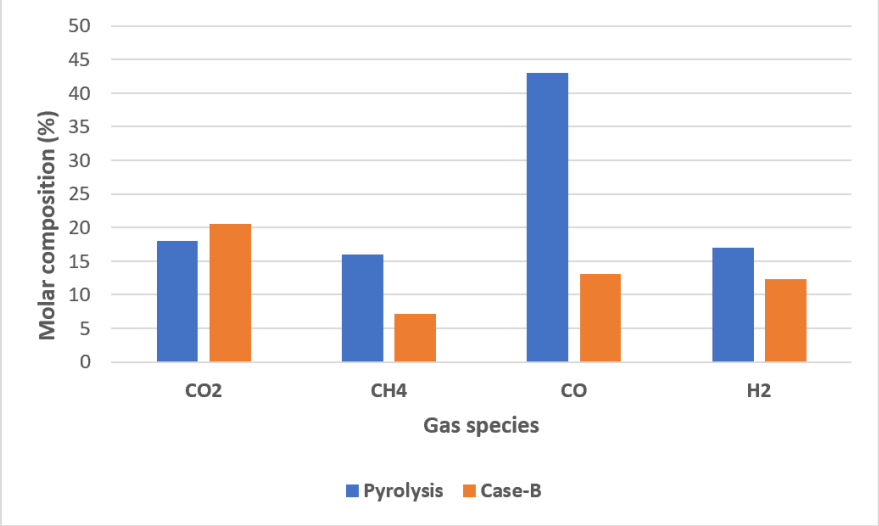

Figure 6.14 Case-B: Input pyrolysis gas composition compared to synthesis gas composition.

Table 6.1 shows the average gas composition from the simulation of the three cases and experimental results. Figure 6.15 shows a plot of the average gas compositions from the simulation of Case-A and B compared with the experimental results. It should be noted that only Case-A and B are comparable with the experimental results, as they have the same reactor temperature. Comparing Case-A and Case-B with the experimental results, both cases gave a good agreement with experimental results in the case of CH_4 and H_2. Case-B gave a closer prediction on CO_2 and CO, which is not as expected because Case-B uses the pyrolysis gas composition for 700°C. This might be due to the tar that was defined in Case-B. However, in both cases, the concentration of CO_2 was overestimated, the concentration of CO was underestimated while the concentration of CH_4 was slightly overestimated.

The overestimation of CO_2 and underestimation of CO might be due to some errors in the pyrolysis gas composition or high rates in the water-gas-shift reaction (2.12) where CO is consumed, and more CO_2 is produced. However, there can also be some experimental uncertainties in measuring the gas composition, related to the GC measurements and during sampling. In the experiment, the biomass feeding was not continuous in contrast to simulation. As the pyrolysis gas composition highly affects the final syngas composition, discontinuous feeding might cause alterations in the actual measured value. In the simulation, it is possible to take a wide range of measurements while in experiments is limited.

However, the deviation between experiment and simulation cannot be avoided. This is mainly because the reaction network is decreased, devolatilization is simplified and the tar generation is minimized or ignored.

Table 6.1 Average gas composition (mole basis) from the simulated cases and experiment.

	Case-A	**Case-B**	**Case-C**	**Experiment**
CO_2	24.1	20.6	22.82	14
CH_4	7	7.1	6.5	4
CO	10	13.1	12.4	19
H_2	14.8	12.3	16.4	17

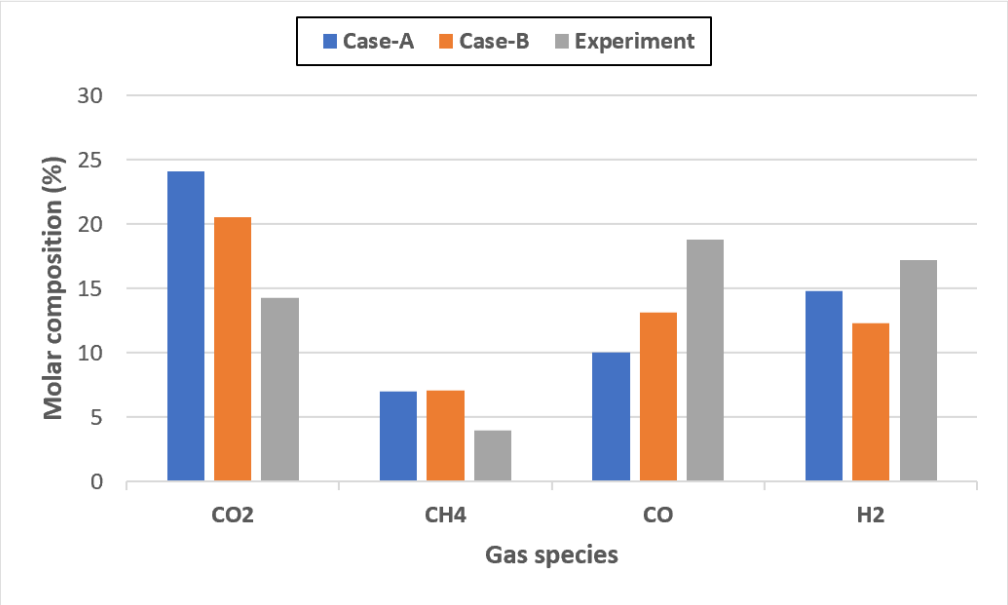

Figure 6.15 Average product gas composition from the three cases compared to the experimental results.

Case-A and C are both compared with each other to study the effect of temperature in synthesis gas composition. As both cases are defined with the same pyrolysis gas composition but different temperatures. Figure 6.16 shows product gas composition from Case-A and Case-B with varying the reactor temperature. Increasing the temperature from 800°C to 900°C, increased the concentration of CO and H_2 while decreased the concentration of CO_2 and CH_4. The CO concentration increased from 10% to 12.4%, CO_2 concentration decreased from 24.1% to 22.8%, CH_4 concentration decreased slightly from 7% to 6.5% and H_2 concentration increased from 14.8% to 16.4%. This is mainly due to the reactions that are enhanced with increasing temperature including, char partial oxidation reaction (3.1), water gas shift reaction (2.12), and the Boudouard reaction (2.8). Higher temperature enhances the tar cracking reactions, resulting in a higher concentration of H_2 and CO. Further, the reactor temperature has a significant effect on the pyrolysis product yields, especially the gas. Therefore, increasing the reactor temperature contributes to higher gas composition and lower tar yields. However, the trends show a good agreement with literature and other experiments except for the trend of CH_4. This might be due to the neglect of the tar composition in the volatiles.

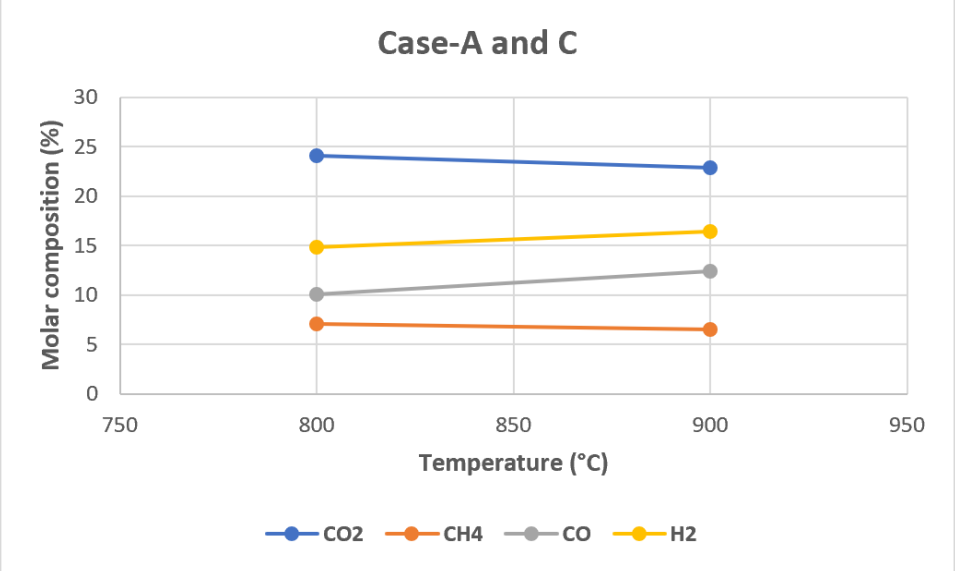

Figure 6.16 Product gas molar fraction for Case-A and Case-B at different temperatures.

6.3 Further work

The pyrolysis experimental unit is newly built, hence some operational problems appeared during the experiments. Several modifications and recommendations can be applied to the pyrolysis unit to improve its performance. They are listed as follows along with some suggestions for the CPFD simulation.

- The pyrolysis reactor must be improved, as one of the main problems was the leakage from the closing flange. To overcome this problem, it is suggested to modify the feeding system, for example by installing a valve or a screw conveyor.
- Improve the condenser unit, as it was observed that the water-cooled condenser did not collect the condensable material properly. However, a set of impinger bottles filled with isopropanol solvent and installed in a cooling bath might improve the condensations.
- When the impinger bottles were used for the experiment, the product gas could not pass through the solvent in the condenser due to pressure. Therefore, it is suggested to use a pump that might be installed after the condenser or along with the N_2 flow input to the reactor.
- An electrical heater instead of a muffle furnace might facilitate the biomass feeding issues and other operational problems.
- Install a new column for the GC. There might be some blockages in the current column due to dust, as the gas samples are injected without being filtered.
- Check the possibilities of installing a flame ionization detector (FID) in the CG, to analyze other hydrocarbons such as ethane.
- Perform pyrolysis experiments with different operational conditions such as temperature, heating rates, biomass size, and the type and study the effects on the product yields.
- Analyze the chemical compositions of biomass, which can be useful to study the effects of different chemical compositions on product yields.

- Include the formation and decomposition of tar in the CPFD simulations. Neglection of this parameter might give errors in the results.

7 Conclusion

The overall aim of this thesis was to design and construct a pyrolysis reactor and perform experimental tests to study the product composition as a function of biomass type and operational conditions, especially the temperature. An extensive literature study has been carried out on the pyrolysis of biomass along with the effects of different operational conditions on the product yields. Another aim was to simulate a fluidized bed gasification reactor using actual experimental data from pyrolysis as input and study the effect of the pyrolysis step on the synthesis gas.

A pyrolysis reactor was designed and constructed, and the pyrolysis experiments were carried out using a muffle furnace. Due to technical reasons, only one experiment with good results was successful. The pyrolysis experimental unit includes, muffle furnace, reactor, water-cooled condenser, nitrogen supply, rotameter, and a gas chromatographer (GC) used to analyze the product gas. The experiment was performed using wood pellets as the feedstock and the reactor temperature was set to 500°C. The product yields were found to be 29.2%, 22.5%, and 48.3% for char, tar, and gas, respectively. There were no studies found on pyrolysis of wood pellets at 500°C and therefore, the results were further compared to pyrolysis of wood experiment obtained from the literature. The char yield was within the range compared to the literature, while the tar yield was lower, and the gas yield was significantly higher. The high gas yield and low tar yield in the experimental results are mainly due to escaping of some of the condensable tar with the gas. The average product gas compositions were found to be 62%, 6.7%, and 33.1% for cumulative CH_4 and CO, H_2, and CO_2, respectively. The experimental gas composition seems to agree well with the results from the literature, especially for H_2 and CO_2.

Computational particle fluid dynamic (CPFD) simulations were carried out to study the composition of the synthesis gas obtained from the air gasification of wood pellets. The model was developed in Barracuda and uses a three-dimensional multiphase particle-in-cell approach. The gasification reactions and reaction rates were defined in the chemistry module. A geometry with 8.83 cm square cross-section and 100 cm height was created. The fractions of the volatiles and the solid from pyrolysis of wood pellets obtained from the literature were used as inputs. Three simulation cases were created by varying the temperature and the pyrolysis gas compositions.

In all cases, the production of CO_2 was highest, and then comes H_2, CO, and CH_4, respectively. The effect of the pyrolysis step on synthesis gas composition was found to be significant, especially on the production of CO, H_2, and CH_4. This is mainly due to the 85% by weight of the synthesis gas was produced during the pyrolysis of biomass step.

Comparing Case-A and B with experimental data showed a good agreement on predicting CH_4 and H_2 while overestimation of CO_2 and underestimation of CO were observed. The deviation of CO_2 and CO might be due to errors in the pyrolysis gas composition or high rates in water-gas shift reaction. Including the decomposition of tar in the simulation seems to give better prediction performance, especially on predicting CO_2 and CO.

The effect of temperature was established by comparing Case-A and C, where the temperature was varied from 800°C up to 900°C. Increasing the temperature increased the concentration of CO and H_2 by 2.4% and 1.6% respectively and decreased the concentration of CO_2 and CH_4 by 1.3% and 0.5% respectively. The trends showed a good agreement with other experiments

from the literature, except the trend of CH_4. This might be due to the neglect of the tar compositions in the volatiles.

References

[1] S. Kaza, L. Yaw, P. Bhada-Tata og F. V. Woerden, What a Waste, Washington: Inernational Bank for Reconstruction and development, 2018.

[2] C. Ellis, «World Bank: Global waste eneration could increase by 70% by 2050,» Industy Dive, 2018.

[3] European Commission , «Directive 2008/98/EC on waste (Waste Framework Directive),» European Commission website, [Internett]. Available: https://ec.europa.eu/environment/waste/framework/. [Funnet 06 02 2021].

[4] I. Barret, «Waste Hierarchy,» European Parliamentary Research Service Blog, 16 03 2016. [Internett]. Available: https://epthinktank.eu/2017/05/29/circular-economy-package-four-legislative-proposals-on-waste-eu-legislation-in-progress/waste_hierarchy/. [Funnet 06 02 2021].

[5] J. S. Tumuluru, «Biomass Compositional Analysis for Conversion to Renewable Fuels and Chemicals,» i *Biomass Volume Estimation nad Valorization for energy*, Idaho, Intechopen, 2017.

[6] X. Hu og M. Gholizadeh, «Biomass pyrolysis: A review of the process development and challenges from initial researches up to the commercialisation stage,» *Energy Chemistry*, vol. 39, pp. 109-143, 2019.

[7] UngEnergi, «Pyrolyse,» UngEnergi, 13 09 2019. [Internett]. Available: https://ungenergi.no/energikilder/bioenergi/pyrolyse/. [Funnet 26 03 2021].

[8] A. Demirbas, «Pyrolysis of Biomass for Fuels and Chemicals,» *Energy Sources,* vol. 31, nr. 12, pp. 1028-1037, 2009.

[9] M. Taherzdeh, K. Bolton, J. Wong og A. Pandey, Sustainable Resource Recovery and Zero Waste Approaches, St. Louis: Elsevier, 2019.

[10] P. H. Bunner og H. Rechberger, «Waste Mabagement,» *Elsevier,* vol. 37, nr. Waste to Energy processes and Technologies, pp. 3-12, 2015.

[11] R. Leblanc, «Waste Treatment and Disposal Methods,» Thebalancesmb, 09 05 2019. [Internett]. Available: https://www.thebalancesmb.com/waste-treatment-and-disposal-methods-2878113. [Funnet 01 02 2021].

[12] H. B. Goyal, D. Seal og R. C. Saxena, «Bio-fuel from thermochemical conversion of renewable resources: A review,» *Elsevier,* vol. 12, nr. 2, pp. 504-517, 2008.

[13] Z. Luo og J. Zhou, «Thermal Conversion of Biomass,» i *Handbook of Climate Change Mitigation*, New York, Springer, 2012, pp. 1001-1042.

[14] P. T. Williams, Waste Treatment and Disposal, 2nd red., Chichester: John Wiley and Sons, Ltd, 2005.

[15] B. Barrows, «What are "Conversion Technologies",» Oregon Department of Environmental Quality, Oregon, 2011.

[16] M. Faizal, Y. H. Wardah, M. A. Husna og Y. H. Tan, «Energy,economic and environmental impact of watse to energy in Malaysia,» *Journal of Mechanical Engineering Research and Developments,* vol. 41, nr. 3, pp. 97-101, 2018.

[17] L. Castrillon, Y. Fernandez-Nava, M. Ulmanu, I. Anger og E. Maranon, «Waste Management,» *Elsevier,* vol. 30, nr. 2, pp. 228-235, 2010.

[18] Alternativ Energy Tutorials, «Biomass Resources,» Alternativ Energy Tutorials, 03 2015. [Internett]. Available: https://www.alternative-energy-tutorials.com/biomass/biomass-resources.html. [Funnet 03 2021].

[19] L. Rosendahl, Biomass Combustion Science, Technology and Engineering, Sawston: Woodhead Publishing Limited, 2013.

[20] T. Govil, J. Wang, D. Samanta, A. David, A. Tripathi, S. Rauniyar, D. R. Salem og R. K. Sani, «Lignocellulosic feedstock: A review of a sustainable platform for cleaner production of nature's plastics,» *Journal of Cleaner Production,* vol. 270, 2020.

[21] T. Kan, V. Strezov og T. J. Evans, «Lignocellulosic biomass pyrolysis: A review of product properties and effect of pyrloysis parameters,» *Renewable and Sustainable Energy Reviews,* vol. 57, pp. 1126-1140, 2016.

[22] P. Basu, Biomass Gasification, Pyrolysis and Torrefaction, 2nd red., London: Elsevier, 2013.

[23] S. L. Suib, New and Future Developments in Catalysis, Connecticut: Elsevier, 2013.

[24] K. Kositkanawuth, M. L. Sattler og B. Dennis, «Pyrolysis of Macroalgae and Polysytrene:A Review,» *Current Sustainable/Renewable Energy Reports,* vol. 1, pp. 121-128, 2014.

[25] S. Sinha, A. Jhalani, M. R. Ravi og A. Ray, «Modeling of pyrolysis wood: A review,» Department of Mechanical Engineering, Indian Institute of Technology, New Delhi, 2000.

[26] P. Tanger, J. L. Field, C. E. Jahn, M. W. Defoort og J. E. Leach, «Biomass for thermochemical conversion: target and chalenges,» frontiers in plant scince, Hazen, 2013.

[27] C. Z. Zaman, K. Pal, W. A. Yehye, S. Sagadevan, S. T. Shah, G. Abimbola, E. Marliana, R. F. Rafique og R. B. Johan, Pyrolysis: a sustainable way to generate energy from waste, Cairo: IntechOpen, 2017.

[28] J. F. Puna og M. T. Santos, «Thermal Conversion Technologies for Solid Wastes: A New Way to Produce Sustainable Energy,» i *Waste Management*, Intch open acces journals, 2014, pp. 132-147.

[29] S. Wang, G. Dai, H. Yang og Z. Luo, «Lignocellulosic biomass pyrolysis mechanism: A state-of-the-art review,» i *Progress in Energy and Combustion Science*, Wuhan, Elsevier, 2017, pp. 33-86.

[30] A. Gabra, «Biomass Conversion Technologies for Bioenergy Generation: An Introduction,» Intechopen, Katsina, 2020.

[31] C. R. Lohri, S. Diener, I. Zabaleta, A. Mertenat og C. Zurbrugg, «Treatment technologies for urban solid biowaste to create value products: A review with focus on low- and middle-income settings,» *Reviews in Environmental Science and Bio/Technology*, vol. 16, pp. 81-130, 2017.

[32] M. I. Jahirul, M. G. Rasul, A. A. Chawdhury og N. Ashwath, «Biofuels Production through Biomass Pyrolysis - A Technological Review,» *Energies*, vol. 5, pp. 4952-5001, 2012.

[33] D. Mallick, P. Mahanta og V. Moholkar, «Co-gasification of coal and biomass blends: Chemistry and engineering,» *Fuel*, vol. 207, pp. 106-128, 2017.

[34] M. Balat, «Mechanisms of Thermochemical Biomass Conversion Processes. Part 1: Reactions of Pyrolysis,» *Energy Sources*, vol. 30, nr. 7, pp. 620-635, 2008.

[35] D. Mohan, C. U. Pittman og P. H. Steele, «Pyrolysis of Wood/Biomass for Bio-oil: A Critical Review,» *Energy&Fuels*, vol. 20, nr. 3, pp. 848-889, 2006.

[36] L. Santamaria, M. Beirow, F. Mangold, G. Lopez, M. Olazar, M. Schmid, Z. Li og G. Scheffknecht, «Influence of temperature on products from fluidized bed pyrolysis of wood and solid recovered fuel,» *Fuel*, vol. 283, 2021.

[37] L. Fagbemi, L. Khezami og R. Capart, «Pyrolysis products from different biomasses: application to the thermal cracking of tar,» *Applied Energy*, vol. 69, nr. 4, pp. 293-306, 2001.

[38] A. K. Hossain og P. A. Davis, «Pyrolysis liquids and gases as alternative fuels in internal combustion engines - A review,» *Renewable and Sustainable Energy Reviews*, vol. 21, pp. 165-189, 2013.

[39] P. Abhijeet, G. Swagathnath, S. Rangabhashiyam, M. Asok Rajkumar og P. Balasubramanian, «Prediction of pyrolytic composition and yield for various grass biomass feedstocks,» *Biomass Conversion and Biorefinery*, vol. 10, pp. 663-674, 2020.

[40] R. A. Moghadam, S. Yusup, W. Azlina, S. Nehzati og A. Tavasoli, «Investigation on syngas production via biomas conversion through the integration of pyrolysis and air-steam gasification process,» *Energy Conversion and Management*, vol. 87, pp. 670-675, 2014.

[41] J. G. Speight, Heavy Oil Recovery and Upgrading, Laramie: Elsevier, 2019.

[42] P. Lahijani, Z. A. Zainal, M. Mohammadi og A. R. Mohamed, «Conversion of the greenhouse gas CO2 to the fuel gas CO via the Boudourad reaction: A review,» *Renewable and Sustainable Energy Reviews,* vol. 41, pp. 615-642, 2015.

[43] D. Choi, J. I. Oh, J. Lee, E. E. Kown og K. Baek, «Compostional modification of products from Co-Pyrolysis of chicken manure and biomass by shifting carbon distribution from pyrolytic oil to syngas using CO2,» *Energy,* vol. 153, pp. 530-538, 2018.

[44] N. Laosiripojana og S. Assabumrungrat, «Catalytic dry reforming of methane over high surface area ceria,» *Applied Catalysis B: Environmental,* vol. 60, nr. 1-2, pp. 107-116, 2005.

[45] M. Usman, W. W. Daud og H. F. Abbas, «Dry reforming of methane: Influence of process parameters - A review,» *Renewable and Sustainable Energy Reviews,* vol. 45, pp. 710-744, 2015.

[46] M. Mbodji, J. M. Commenge, L. Falk, D. D. Marco, F. Rossingol, L. Prost, S. Valentin, R. Joly og P. Del-Gallo, «Steam reforming reaction process intensification by using a millistructed reactor: Experimental setup and model validation for global kinetic reaction rate estimation,» *Chemical Engineering Journal,* Vol. %1 av %2207-208, pp. 871-884, 2012.

[47] C. Wheeler, A. Jhalani, E. J. Klein, S. Tummala og L. D. Schmidt, «The water-gas-shift reaction at short contact times,» *Journal of Catalysis,* vol. 223, nr. 1, pp. 191-199, 2004.

[48] F. Mashkani og M. Razaei, «Simplified direct pyrolysis method for preparation of nanocrystalline iron based catalysts for H2 purificationvia high temperature water gas shift reaction,» *Chemical Engineering Researsch and Design,* vol. 95, pp. 288-297, 2015.

[49] J. G. Speight, «Gasification reaction kinetics for synthetic liquid fuel production,» i *Gasification for Synthetic Fuel Production,* Laramie, Elsevier , 2015, pp. 103-117.

[50] F. Meshkani og M. Razaei, «High temperature water gas shift reaction over promoted iron based catalysts prepared by pyrolysis method,» *International Journal of Hydrogen Energy,* vol. 39, nr. 29, pp. 16318-16328, 2014.

[51] A. Hlavsova, A. Carsaro, H. Raclavska, D. Jachelkova, H. Skrobankova og J. Frydrych, «Syngas production from pyrolysis of nine composts obtained from nonhybrid and hybrid Perennial grasses,» *The Scientific World Journal,* vol. 2014, p. 11, 2014.

[52] A. Demirbas, «Effect of Temperature on Pyrolysis Products from Biomass,» *Energy Sources,* vol. 29, nr. 4, pp. 329-336, 2007.

[53] E. Salehi, J. Abedi og T. Harding, «Bio-oil from Sawdust: Pyrolysis of Sawdust in a Fixed-Bed System,» *Energy & Fuels,* vol. 23, nr. 7, pp. 3767-3772, 2009.

[54] D. Chen, J. Zhou og Q. Zhang, «Effect of heating rate on slow pyrolysis behavior, kinetic parameters and product properties of moso bamboo,» *Bioresource Technology,* vol. 169, pp. 313-319, 2014.

[55] K. K. Zaman, V. Balasundram, N. Ibrahim, M. D. Muhaimin, R. M. Kasmani, M. K. Abd Hamid og H. Hasbullah, «Effect of Particle Size and Temperature on Pyrolysis of Paalm Kernel Shell,» *International Journal of Engineering & Technology,* vol. 7, nr. 4.35, pp. 118-124, 2018.

[56] A. Monilo, S. Chianese og D. Musmarra, «Biomass gasification technology: The state of the art overview,» *Journal of Energy Chemistry,* vol. 25, nr. 1, pp. 10-25, 2016.

[57] J.-P. Badeau og A. Levi, Biomass Gasification: Chemistry, Process and Aplications, New York: Nova Science Publishers, 2009.

[58] K. Sun, «Optimization of biomass gasification reactor using Aspen Plus,» Telemark University College, Nøtterøy, 2014.

[59] A. Gomez-Barea og B. Leckner, «Modeling of biomass gasification in fluidized bed,» *Progress in Energy and Combustion Science,* vol. 36, nr. 4, pp. 444-509, 2010.

[60] CPFD Software, «Complements Other Tools,» 2021. [Internett]. Available: https://cpfd-software.com/technology/complements-other-tools/.

[61] K. Sun, «Optimization of biomass gasification reactor using Aspen Plus,» Telemark University College, Porsgrunn, 2014.

[62] M. B. Nikoo og N. Mahinpey, «Simulation of biomass gasification in fluidized bed reactor using ASPEN PLUS,» *Biomass and Bioenergy,* vol. 32, nr. 12, pp. 1245-1254, 2008.

[63] Technology Evaluation Centers, «The Computational Fluid Dynamics (CFD) Software,» TEC, 2021. [Internett]. Available: https://www3.technologyevaluation.com/c/computational-fluid-dynamics-cfd#:~:text=Computational%20fluid%20dynamics%20(CFD)%20software%20brings%20the%20testing%20of%20flow,of%20safety%20and%20structural%20integrity.. [Funnet 2021].

[64] X. Ku, T. Li og T. Løvås, «CFD-DEM simulation of biomass gasification with steam in a fluidized bed reactor,» *Chemical Engineering Science,* vol. 122, pp. 270-283, 2015.

[65] J. Bandara, «Simulation and parameter optimization of fluidized-bed and biomass gasification,» Univercity of South-Eastern Norway, Porsgrunn, 2021.

[66] M. Chrigui, «Eulerian-Lagrangian Approach for Modeling and Simulation of Turbulent Reactive Multi-Phase Flows under Gas Turbine Combutor Conditions,» Technische Univeritat Darmstadt, Darmstadt, 2005.

[67] «CPFD Software Realeases Barracuda Virtual Reactor 17.4,» CPFD Software LLC, 26 03 2019. [Internett]. Available: https://cpfd-software.com/news/cpfd-software-releases-barracuda-virtual-reactor-17.4. [Funnet 03 05 2021].

[68] C. K. Perera, «Optimization of biomass gasification reactor,» Telemark Univercity College, Porsgrunn, 2013.

[69] R. Jaiswal, «Computational modeling and experimental studies on fluidized bed regimes,» University of South-Eastern Norway, Porsgrunn, 2018.

[70] J. Dong, Y. Chi, Y. Tang, N. Ni, A. Nzihou, E. W. Hortala og Q. Huang, «Effect of operating parameters and moisture content on Municipal solid waste pyrolysis and gasification,» *Energy and fuels*, vol. 30, nr. 5, pp. 2994-4001, 2016.

[71] S. Xiong, J. Zhuo, B. Zhang og Q. Yao, «Effect of moisrure content on the characterization of products from the pyrolysis of sewage sludge,» *Analytical and Applied Pyrolysis*, vol. 104, pp. 632-639, 2013.

[72] BioEnergy Consult, «Biomass As Renewable Energy Resource,» Bioenergy Consult, 08 25 2020. [Internett]. Available: https://www.bioenergyconsult.com/biomass-resources/. [Funnet 03 03 2021].

Appendices

Appendix A: Task description

University of South-Eastern Norway

Faculty of Technology, Natural Sciences and Maritime Sciences, Campus Porsgrunn

FMH606 Master's Thesis

Title: Pyrolysis of biomass

USN supervisor: Britt M. E. Moldestad, Janitha Bandara, Hildegunn H. Haugen

Task background:

Pyrolysis of biomass is considered to be a green technology and has no adverse effects or emissions to the environment. Pyrolysis is the thermal decomposition of biomass occurring in the absence of oxygen, and is a step in both the combustion and gasification processes. The products of biomass pyrolysis include biochar, bio-oil and gases including methane, hydrogen, carbon monoxide, and carbon dioxide. The proportion of these products depends on the composition of the feedstock and the process parameters. In this project, the focus will be on the product gas. It is important to obtain a set of gas composition data from different types of biomass. The data will be used as input to a software to be used for simulation of biomass pyrolysis and gasification. The data will also to be used for design of a lab scale pyrolysis reactor.

Task description:

1. Literature study
    a. Pyrolysis of biomass
        i. Report/find data from proximate and ultimate analysis of biomass
        ii. Report/find data about composition of product gas from pyrolysis of different types of biomass.
        iii. Products: Char, oil, gas. Typical fraction of the products.
    b. Fluidized bed pyrolysis reactor
    c. Simulation of pyrolysis processes
2. Experimental tests to study the pyrolysis products. The experiments will be carried out in a muffle furnace and will be performed with:
    a. Different types and sizes of biomass
    b. Different temperatures

    The product gas will be analysed with respect to composition.
3. Simulation of fluidized bed pyrolysis/gasification reactor
4. Designing and construction of a pyrolysis reactor

Student category: EET and PT students

The task is suitable for online students (not present at the campus): No

Practical arrangements:
Experiments and simulations will be performed at USN.

Supervision:
As a general rule, the student is entitled to 15-20 hours of supervision. This includes necessary time for the supervisor to prepare for supervision meetings (reading material to be discussed, etc).

Appendix B: Wood pellets analysis

Eurofins Environment Testing Norway
AS (Moss)
F. reg. NO9 651 416 18
Møllebakken 50
NO-1538 Moss

Tlf: +47 69 00 52 00
Environment_sales@eurofins.no

Universitetet i Sørøst- Norge
Kjølnes ring 56
3918 Porsgrunn
Attn: Nora Furuvik

AR-21-MM-012100-01

EUNOMO-00283414

Prøvemottak: 13.01.2021
Temperatur:
Analyseperiode: 13.01.2021-22.02.2021

Referanse: britth/7300-FLASH

ANALYSERAPPORT

Prøvenr.:	439-2021-01130307	Prøvetakingsdato:	11.01.2021
Prøvetype:	Fast biobrensel Aske	Prøvetaker:	Nora Furuvik
Prøvemerking:	Prøve c (7/9)(8/9)(9/9) Wood-pellets	Analysestartdato:	13.01.2021

	Analyse	Resultat	Enhet	LOQ	MU	Metode
c)	Svovel (S)	<0.011	% tv	0.01		SS 187177:2017, SS-EN ISO 16994:2016 mod, SS-EN 15408:2011, SS 187177 / EN 15289 / EN15408
c)	Svovel (S)	<0.010	%	0.01		SS 187177:2017, SS-EN ISO 16994:2016 mod, SS-EN 15408:2011, SS 187177 / EN 15289 / EN15408
c)	**Askeinnhold inkl askedannere**					
c)	Askeinnhold inkl. askedannere	0.55	% tv	0.1	10%	EN 14775 / EN 15403 / SS 187171, EN 14775:2009, SS-EN 15403:2011, SS-EN ISO 18122:2015
c)	Askeinnhold inkl. askedannere - mottatt prøve	0.51	%	0.1	10%	EN 14775 / EN 15403 / SS 187171, EN 14775:2009, SS-EN 15403:2011, SS-EN ISO 18122:2015
c)	**Effektiv varmeverdi - konstant trykk, askefri, tørr prøve**					
c)	Eff. varmeverdi - konst p, askefritt (tørr prøve)	19.166	MJ/kg		5%	SS-EN ISO 18125:2017, SS-EN ISO 18125:2017, SS-EN 15400:2011, ISO 1928:2020, SS-EN 15400:2011
c)	Eff. varmeverdi - konst p, askefritt (tørr prøve)	4578	kcal/kg		5%	SS-EN ISO 18125:2017, SS-EN ISO 18125:2017, SS-EN 15400:2011, ISO 1928:2020, SS-EN 15400:2011
c)	Eff. varmeverdi - konst p, askefritt (tørr prøve)	5.322	MWh/tonn		5%	SS-EN ISO 18125:2017, SS-EN ISO 18125:2017,

Tegnforklaring:

* Ikke omfattet av akkrediteringen LOQ: Kvantifiseringsgrense MU: Måleusikkerhet
<: Mindre enn >: Større enn nd: Ikke påvist. Bakteriologiske resultater angitt som <1,<50 e.l. betyr 'ikke påvist'.

Måleusikkerhet er angitt med dekningsfaktor k=2. Måleusikkerhet er ikke tatt hensyn til ved vurdering av om resultatet er utenfor grenseverdi/ -området.
For mikrobiologiske analyser oppgis konfidensintervallet. Ytterligere opplysninger om måleusikkerhet fås ved henvendelse til laboratoriet.
Rapporten må ikke gjengis, unntatt i sin helhet, uten laboratoriets skriftlige godkjennelse. Resultatene gjelder kun for de(n) undersøkte prøven(e).
Resultater gjelder prøven slik den ble mottatt hos laboratoriet.

AR-001 v 166

AR-21-MM-012100-01

eurofins

EUNOMO-00283414

					SS-EN 15400:2011, ISO 1928:2020, SS-EN 15400:2011
c)	**Effektiv varmeverdi - konstant trykk**				
c)	Eff. varmeverdi - konst p (mottatt prøve)	17.364	MJ/kg	5%	SS-EN ISO 18125:2017, SS-EN 15400:2011, SS-EN ISO 18125:2017, ISO 1928:2020, SS-EN 15400:2011
c)	Eff. varmeverdi - konst p (mottatt prøve)	4147	kcal/kg	5%	SS-EN ISO 18125:2017, SS-EN 15400:2011, SS-EN ISO 18125:2017, ISO 1928:2020, SS-EN 15400:2011
c)	Eff. varmeverdi - konst p (mottatt prøve)	4.822	MWh/tonn	5%	SS-EN ISO 18125:2017, SS-EN 15400:2011, SS-EN ISO 18125:2017, ISO 1928:2020, SS-EN 15400:2011
c)	Eff. varmeverdi - konst p (tørr prøve)	19.061	MJ/kg	5%	SS-EN ISO 18125:2017, SS-EN 15400:2011, SS-EN ISO 18125:2017, ISO 1928:2020, SS-EN 15400:2011
c)	Eff. varmeverdi - konst p (tørr prøve)	4553	kcal/kg	5%	SS-EN ISO 18125:2017, SS-EN 15400:2011, SS-EN ISO 18125:2017, ISO 1928:2020, SS-EN 15400:2011
c)	Eff. varmeverdi - konst p (tørr prøve)	5.293	MWh/tonn	5%	SS-EN ISO 18125:2017, SS-EN 15400:2011, SS-EN ISO 18125:2017, ISO 1928:2020, SS-EN 15400:2011
c)	**Effektiv varmeverdi, konstant volum**				
c)	Eff. varmeverdi - konst V (mottatt prøve)	17.441	MJ/kg	5%	SS-EN ISO 18125:2017, SS-EN 15400:2011, SS-EN ISO 18125:2017, ISO 1928:2020, SS-EN 15400:2011
c)	Eff. varmeverdi - konst V (mottatt prøve)	4166	kcal/kg	5%	SS-EN ISO 18125:2017, SS-EN 15400:2011, SS-EN ISO 18125:2017, ISO 1928:2020, SS-EN 15400:2011
c)	Eff. varmeverdi - konst V (mottatt prøve)	4.843	MWh/tonn	5%	SS-EN ISO 18125:2017, SS-EN 15400:2011, SS-EN ISO 18125:2017, ISO 1928:2020, SS-EN 15400:2011
c)	Eff. varmeverdi - konst V (tørr prøve)	19.132	MJ/kg	5%	SS-EN ISO 18125:2017, SS-EN

Tegnforklaring:

* Ikke omfattet av akkrediteringen LOQ: Kvantifiseringsgrense MU: Måleusikkerhet

<: Mindre enn >: Større enn nd: Ikke påvist. Bakteriologiske resultater angitt som <1,<50 e.l. betyr 'ikke påvist'.

Måleusikkerhet er angitt med dekningsfaktor k=2. Måleusikkerhet er ikke tatt hensyn til ved vurdering av om resultatet er utenfor grenseverdi/ -området.
For mikrobiologiske analyser oppgis konfidensintervallet. Ytterligere opplysninger om måleusikkerhet fås ved henvendelse til laboratoriet.
Rapporten må ikke gjengis, unntatt i sin helhet, uten laboratoriets skriftlige godkjennelse. Resultatene gjelder kun for de(n) undersøkte prøven(e).
Resultater gjelder prøven slik den ble mottatt hos laboratoriet.

AR-001 v 166

AR-21-MM-012100-01

EUNOMO-00283414

						15400:2011, SS-EN ISO 18125:2017, ISO 1928:2020, SS-EN 15400:2011
c)	Eff. varmeverdi - konst V (tørr prøve)	4570	kcal/kg		5%	SS-EN ISO 18125:2017, SS-EN 15400:2011, SS-EN ISO 18125:2017, ISO 1928:2020, SS-EN 15400:2011
c)	Eff. varmeverdi - konst V (tørr prøve)	5.313	MWh/tonn		5%	SS-EN ISO 18125:2017, SS-EN 15400:2011, SS-EN ISO 18125:2017, ISO 1928:2020, SS-EN 15400:2011
c)	**Effektiv varmeverdi - konstant volum, askefri, tørr prøve**					
c)	Eff. varmeverdi - konst V, askefritt (tørr prøve)	19.238	MJ/kg		5%	SS-EN ISO 18125:2017, SS-EN 15400:2011, SS-EN ISO 18125:2017, ISO 1928:2020, SS-EN 15400:2011
c)	Eff. varmeverdi - konst V, askefritt (tørr prøve)	4595	kcal/kg		5%	SS-EN ISO 18125:2017, SS-EN 15400:2011, SS-EN ISO 18125:2017, ISO 1928:2020, SS-EN 15400:2011
c)	Eff. varmeverdi - konst V, askefritt (tørr prøve)	5.342	MWh/tonn		5%	SS-EN ISO 18125:2017, SS-EN 15400:2011, SS-EN ISO 18125:2017, ISO 1928:2020, SS-EN 15400:2011
c)	Fuktinnhold	7.9	%	0.1	10%	SS-EN 15934:2012 mod., SS-EN 15934:2012 mod., SIS-CEN/TS 15414-2:2014 / SS-EN15414-3:2011, SIS-CEN/TS 15414-2:2014 mod. / SS-EN15414-3:2011 m, SIS-CEN/TS 15414-2:2014 / SS-EN15414-3:2011, SS-EN ISO 18134-2:2017, -3(mod):2015, SS-EN ISO 18134-2:2017, -3(mod):2015
c)	Hydrogen (H)	6.1	% tv	0.1	10%	SS-EN 15407:2011, SS-EN ISO 16948:2015, SS-EN ISO 16948:2015, SS-EN 15407:2011, SS-EN ISO 16948:2015
c)	Hydrogen (H) lev. tilstand	6.5	%	0.1	10%	SS-EN 15407:2011, SS-EN ISO

Tegnforklaring:

* Ikke omfattet av akkrediteringen LOQ: Kvantifiseringsgrense MU: Måleusikkerhet

<: Mindre enn >: Større enn nd: Ikke påvist. Bakteriologiske resultater angitt som <1,<50 e.l. betyr 'ikke påvist'.

Måleusikkerhet er angitt med dekningsfaktor k=2. Måleusikkerhet er ikke tatt hensyn til ved vurdering av om resultatet er utenfor grenseverdi/ -området.
For mikrobiologiske analyser oppgis konfidensintervallet. Ytterligere opplysninger om måleusikkerhet fås ved henvendelse til laboratoriet.
Rapporten må ikke gjengis, unntatt i sin helhet, uten laboratoriets skriftlige godkjennelse. Resultatene gjelder kun for de(n) undersøkte prøven(e).
Resultater gjelder prøven slik den ble mottatt hos laboratoriet.

AR-001 v 166

AR-21-MM-012100-01

eurofins

EUNOMO-00283414

					16948:2015, SS-EN ISO 16948:2015, SS-EN 15407:2011, SS-EN ISO 16948:2015
c)	**Kalorimetrisk varmeverdi**				
c)	Kal. varmeverdi (mottatt prøve)	18.774	MJ/kg	5%	SS-EN 15400:2011, SS-EN ISO 18125:2017, SS-EN ISO 18125:2017, SS-EN ISO 18125:2017, SS-EN 15400:2011, ISO 1928:2020, ISO 1928:2020, ISO 1928:2020
c)	Kal. varmeverdi (mottatt prøve)	4487	kcal/kg	5%	SS-EN 15400:2011, SS-EN ISO 18125:2017, SS-EN ISO 18125:2017, SS-EN ISO 18125:2017, SS-EN 15400:2011, ISO 1928:2020, ISO 1928:2020, ISO 1928:2020
c)	Kal. varmeverdi (mottatt prøve)	5.213	MWh/tonn	5%	SS-EN 15400:2011, SS-EN ISO 18125:2017, SS-EN ISO 18125:2017, SS-EN ISO 18125:2017, SS-EN 15400:2011, ISO 1928:2020, ISO 1928:2020, ISO 1928:2020
c)	Kal. varmeverdi (tørr prøve)	20.382	MJ/kg	5%	SS-EN 15400:2011, SS-EN ISO 18125:2017, SS-EN ISO 18125:2017, SS-EN ISO 18125:2017, SS-EN 15400:2011, ISO 1928:2020, ISO 1928:2020, ISO 1928:2020
c)	Kal. varmeverdi (tørr prøve)	4871	kcal/kg	5%	SS-EN 15400:2011, SS-EN ISO 18125:2017, SS-EN ISO 18125:2017, SS-EN ISO 18125:2017, SS-EN 15400:2011, ISO 1928:2020, ISO 1928:2020, ISO 1928:2020
c)	Kal. varmeverdi (tørr prøve)	5.660	MWh/tonn	5%	SS-EN 15400:2011, SS-EN ISO 18125:2017, SS-EN ISO 18125:2017, SS-EN ISO 18125:2017, SS-EN

AR-21-MM-012100-01

eurofins

EUNOMO-00283414

					15400:2011, ISO 1928:2020, ISO 1928:2020, ISO 1928:2020
c)	Karbon (C)	51.3 % tv	0.1	5%	SS-EN 15407:2011, SS-EN ISO 16948:2015, SS-EN ISO 16948:2015, SS-EN 15407:2011, SS-EN ISO 16948:2015
c)	Karbon (C), lev. tilstand	47.2 %	0.1	5%	SS-EN 15407:2011, SS-EN ISO 16948:2015, SS-EN ISO 16948:2015, SS-EN 15407:2011, SS-EN ISO 16948:2015
b)	Klor (Cl)	<0.011 % tv	0.01		SS-EN 15408:2011, SS-EN ISO 16994:2016, SS-EN 15408:2011, SS 187185:2017
b)	Klor (Cl), lev. tilstand	<0.010 %	0.01		SS-EN 15408:2011, SS-EN ISO 16994:2016, SS-EN 15408:2011, SS 187185:2017
c)	**Nitrogen (N)**				
c)	Total nitrogen (N)	<0.11 % tv	0.1		SS-EN ISO 16948:2015, SS-EN ISO 16948:2015, SS-EN 15407:2011, SS-EN 15407:2011, SS-EN ISO 16948:2015
c)	Nitrogen (N) lev. tilstand	<0.10 %	0.1		SS-EN ISO 16948:2015, SS-EN ISO 16948:2015, SS-EN 15407:2011, SS-EN 15407:2011, SS-EN ISO 16948:2015
c)	Oksygen (beregnet)	42.0 % tv			SS-EN ISO 18125:2017, SS-EN 15400:2011, SS-EN ISO 18125:2017, SS-EN ISO 18125:2017, SS-EN 15400:2011, ASTM D3176-2015, ASTM D3176-2015, ASTM D3176-2015, SS-EN ISO 18125:2017
c)	Oksygen lev. tilstand (beregnet)	45.7 %	0.1		SS-EN ISO 18125:2017, SS-EN 15400:2011, SS-EN ISO 18125:2017, SS-EN ISO 18125:2017, SS-EN 15400:2011, ASTM

AR-21-MM-012100-01

eurofins

EUNOMO-00283414

						540:2008
c)	Krympingstemperatur SST	1230	°C	500	10%	ISO 540:2008, CEN/TS 15404:2014, ISO 21404:2020, ISO 21404:2020, CEN/TS 15404:2014, ISO 540:2008
c)	Deformasjonstemperatur DT	1270	°C	500	5%	ISO 540:2008, CEN/TS 15404:2014, ISO 21404:2020, ISO 21404:2020, CEN/TS 15404:2014, ISO 540:2008
c)	Halvsfærisk temperatur HT	1300	°C	500	5%	ISO 540:2008, CEN/TS 15404:2014, ISO 21404:2020, ISO 21404:2020, CEN/TS 15404:2014, ISO 540:2008
c)	Flytende temperatur FT	1310	°C	500	5%	ISO 540:2008, CEN/TS 15404:2014, ISO 21404:2020, ISO 21404:2020, CEN/TS 15404:2014, ISO 540:2008
c)	Flyktige forbindelser	83.9	% TS	0.2	5%	SS-EN 15402:2011, SS-EN ISO 18123:2015, SS-EN 15402:2011, SS-EN ISO 18123:2015
c)	Flyktige forbindelser, lev. tilstand	77.3	%	0.2	5%	SS-EN 15402:2011, SS-EN ISO 18123:2015, SS-EN 15402:2011, SS-EN ISO 18123:2015
c)	**Forbehandling knusing/kverning**					
c)	Homogenisering, knusing	1.0				SS-EN 15443:2011, SS-EN ISO 14780:2017, SS 187117:1997, SS-EN 15002:2015-07, ISO 18283:2006, ISO 18283:2006, SS-EN 15002:2015-07, SS-EN 15002:2015-07, SS-EN 15002:2015-07, SS-EN 15002:2015-07, SS-EN 15002:2015-07, ISO 11464:2006-12, SS 187114:2017, SS-EN 16179:2012, SS-EN 16179:2012

AR-21-MM-012100-01

EUNOMO-00283414

a)* Eurofins Environment Sweden AB (Lidköping), Box 887, Sjöhagsg. 3, SE-53119, Lidköping
a) Eurofins Environment Sweden AB (Lidköping), Box 887, Sjöhagsg. 3, SE-53119, Lidköping ISO/IEC 17025:2017 SWEDAC 1125,
b) Eurofins Water Testing Sweden, Box 737, Sjöhagsgatan 3, 53119, Lidköping ISO/IEC 17025:2017 SWEDAC 10300,
c)* Eurofins Biofuel &Energy Testing Sweden(Lidköping), Sjöhagsgatan 3, 531 40, Lidköping
c) Eurofins Biofuel &Energy Testing Sweden(Lidköping), Sjöhagsgatan 3, 531 40, Lidköping ISO/IEC 17025:2017 SWEDAC 1820,

Moss 22.02.2021

Kjetil Sjaastad

Kjetil Sjaastad

Analytical Service Manager

Appendix C: Safety issues and concerns for pyrolysis experiments

This is a newly built pyrolysis unit and therefore, there was operation problems. It is important to follow the safety issues listed below:

- The biomass sample is introduced to a heated oven. Therefore, it is necessary to have extra concerns. Temperature resistant gloves should be wore always.
- The pyrolysis unit was place inside the chimney so that any leakage will encounter with the user.
- Use maximum 50 grams of sample for the experiments that it will not generate large amounts of gases at once.
- Always check the nitrogen pressure and make sure that the nitrogen flow in the reactor is at least at 0.1 L/min.
- Fully tight all the bolts at the closure flange.
- Make sure that all the attachments from the reactor out to the condenser are properly fixed.
- Any leakage can be observed by gas coming out the furnace door or two exits from the furnace back.
- If any leakage is observed, do not open the furnace door, and wait until the pyrolysis is completed (can be observed when there is not any smoke inside the condenser).
- The furnace must be cooled down to at least 200 ºC before leaving the unit.
- Make sure that the chimney fan is working.

Appendix D: Gas chromatograph analysis

After 2 minutes

Component	Datalogger	Retention	Area	Height	External	Unit
Oxygen	26.886	1.486	39.7880	7.845	0.2257	%
Nitrogen	26.886	1.726	14971.1789	963.583	81.3585	
Carbon monoxide	26.886	3.493	635.8450	43.418	2.3853	%
CO2	26.886	9.393	2408.1506	140.145	9.3048	
			18054.9625		93.2744	

After 4 minutes

Component	Datalogger	Retention	Area	Height	External	Units	Units	Norm area %
Oxygen	22.142	1.556	33.3782	6.573	0.1893	%	%	0.1573
Nitrogen	22.142	1.836	5861.2758	559.670	31.8522			26.4684
Methane	22.142	3.246	4660.9228	281.077	50.4283			41.9047
CO2	22.142	9.153	9801.1624	445.917	37.8707			31.4696
			20356.7392		120.3405			100.0000

After 7 minutes

Component	Datalogger	Retention	Area	Height	External	Units	Units	Norm area %
Oxygen	23.010	1.623	94.4164	18.419	0.5356	%	%	0.4084
Nitrogen	23.010	1.936	1516.4744	216.391	8.2410			6.2850
Methane	23.010	3.173	7035.2258	366.631	76.1168			58.0506
CO2	23.010	9.110	11964.1112	512.270	46.2281			35.2559
			20610.2278		131.1215			100.0000

After 8 minutes

Component	Datalogger	Retention	Area	Height	External	Units	Units	Norm area %
Oxygen	1.580	1.620	24.2244	4.683	0.1374	%	%	0.1024
Nitrogen	1.580	1.933	1621.5807	233.469	8.8122			6.5644
Methane	1.580	3.170	7707.3710	434.241	83.3890			62.1178
CO2	1.580	9.130	10845.2037	477.738	41.9047			31.2155
			20198.3798		134.2434			100.0000

After 9 minutes

Component	Datalogger	Retention	Area	Height	External	Units	Units	Norm area %
Oxygen	0.947	1.616	45.9364	9.182	0.2606	%	%	0.1899
Nitrogen	0.947	1.930	1589.1366	228.309	8.6359			6.2953
Methane	0.947	3.140	9041.8177	510.161	97.8269			71.3127
CO2	0.947	9.200	7882.4102	379.061	30.4568			22.2020
			18559.3009		137.1802			100.0000

After 2 minutes

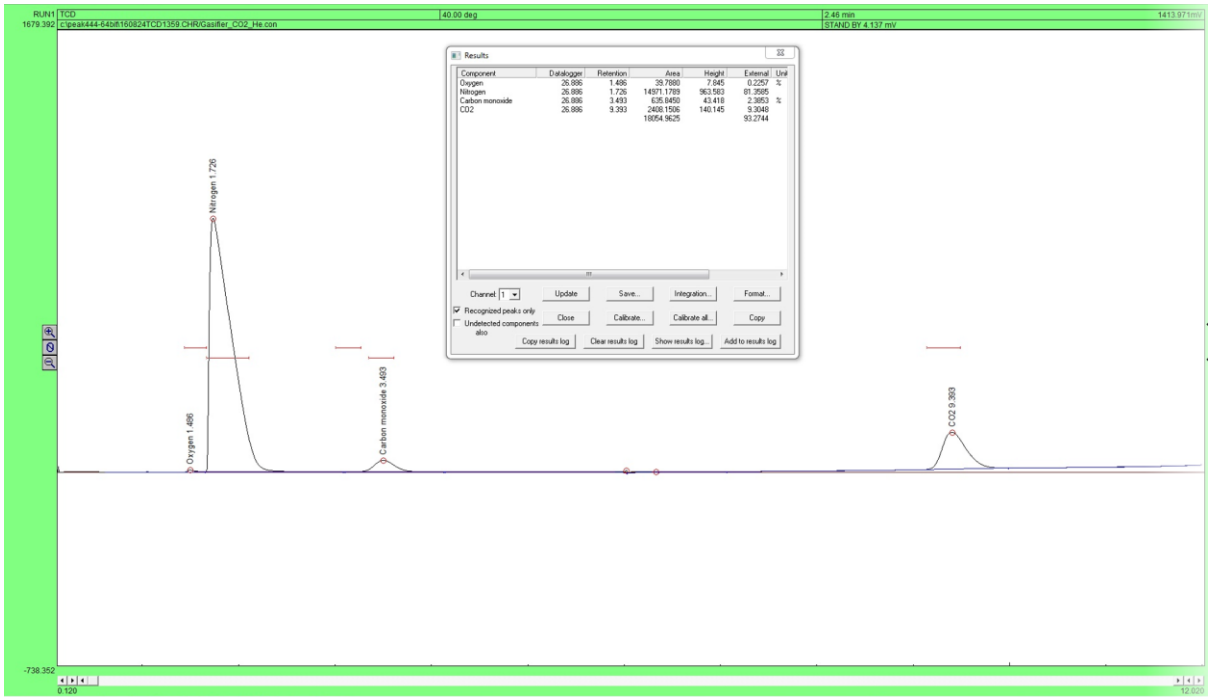

After 4 minutes

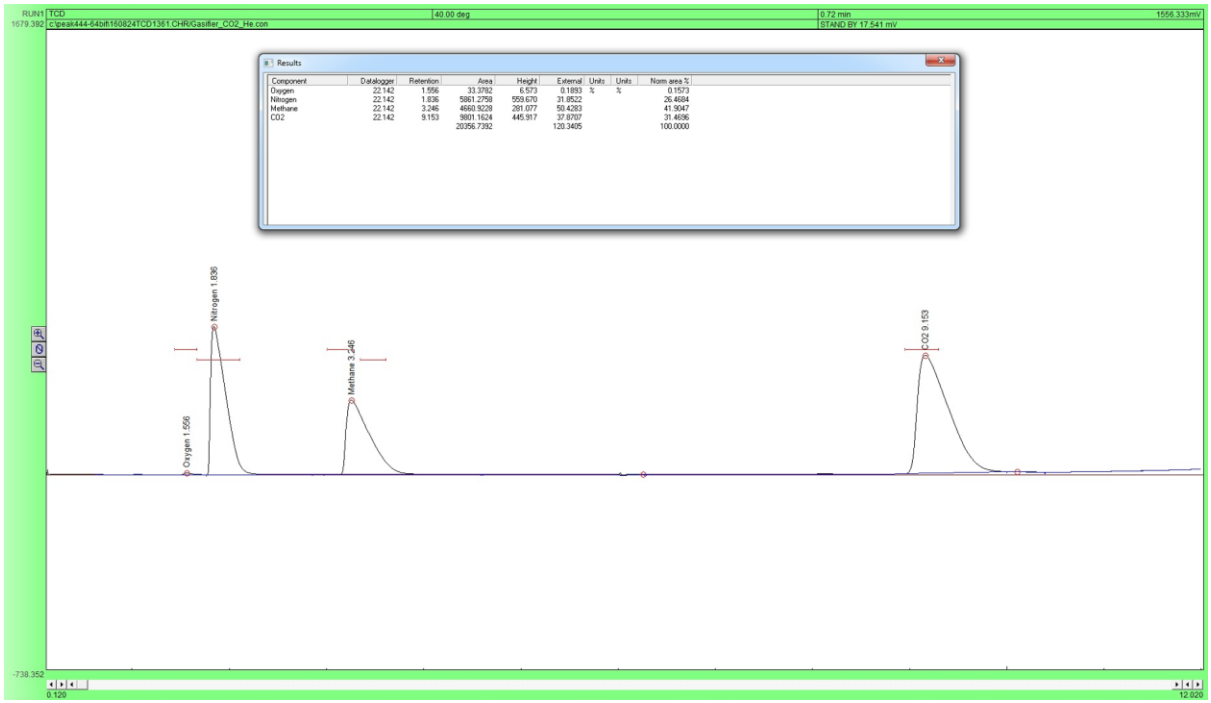

After 7 minutes

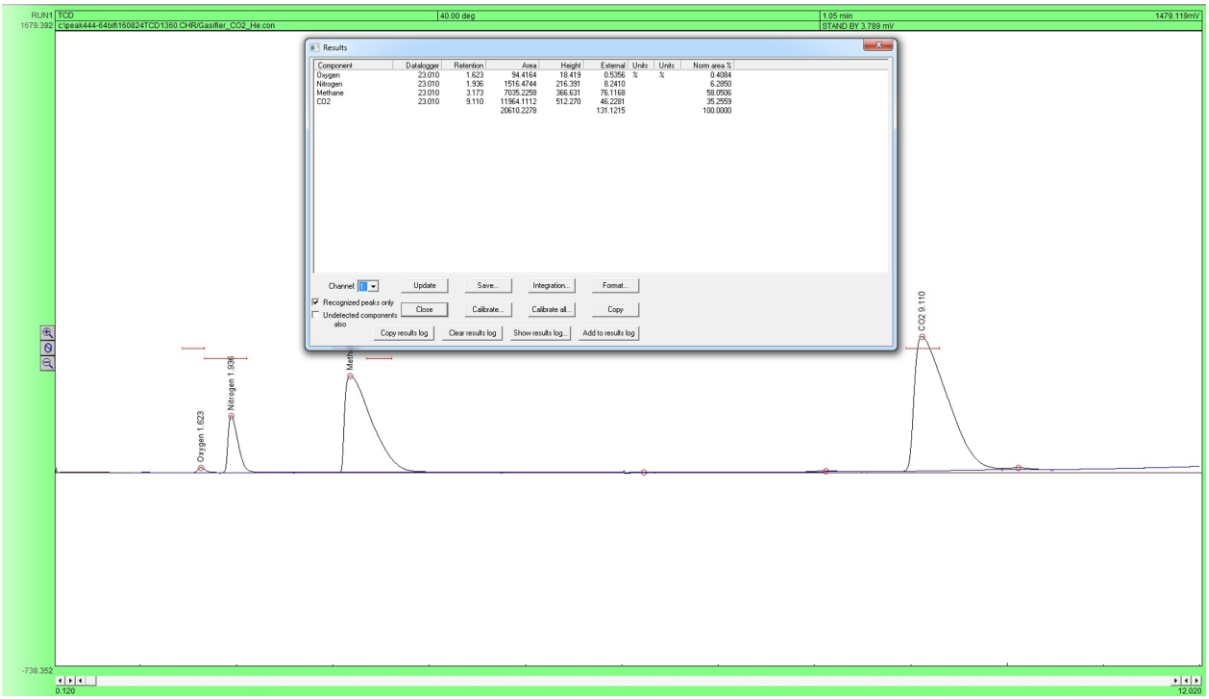

After 8 minutes

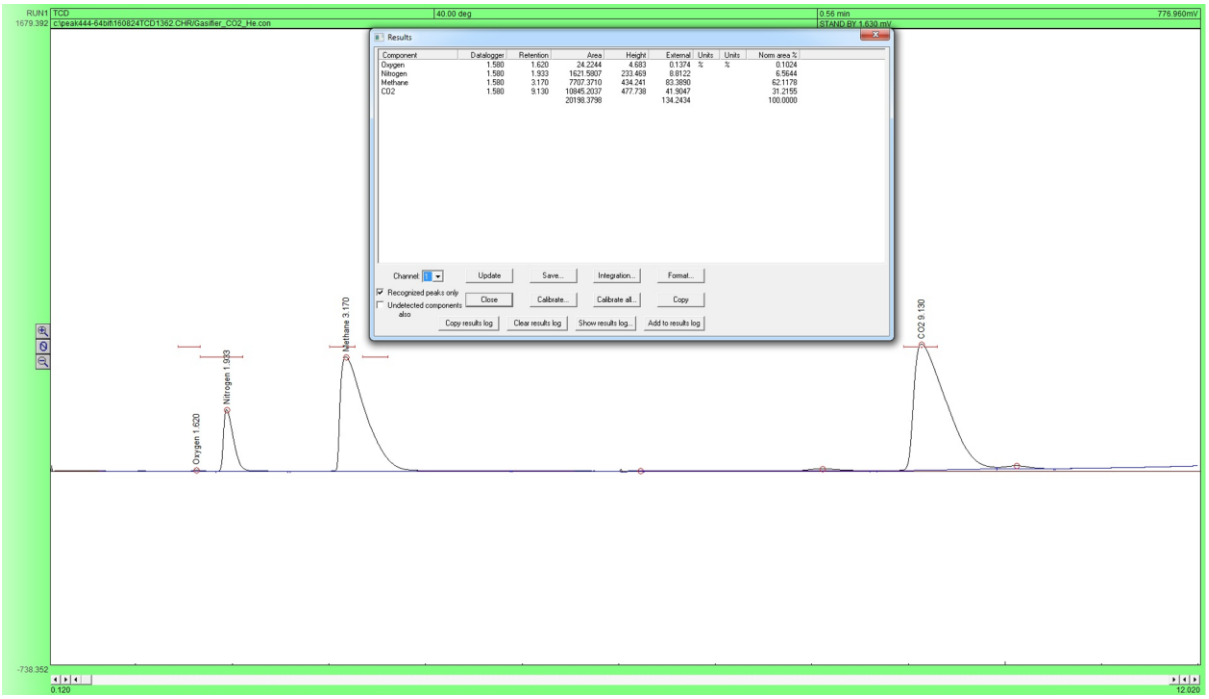

After 9 minutes